

Uncertainties and understanding of experimental and theoretical results regarding reactions forming heavy and superheavy nuclei

G. Giardina^a, G. Mandaglio^{b,c}, A.K. Nasirov^{d,e}, A. Anastasi^{a,f}, F. Curciarello^f, G. Fazio^a

^a*Dipartimento di Scienze Matematiche e Informatiche, Scienze Fisiche e Scienze della Terra, University of Messina, Messina, Italy*

^b*Dipartimento di Scienze Chimiche, Biologiche, Farmaceutiche ed Ambientali, University of Messina, Messina, Italy*

^c*INFN Sezione di Catania, Catania, Italy*

^d*JINR - Bogoliubov Laboratory of Theoretical Physics, Dubna, Russia*

^e*Institute of Nuclear Physics Uzbek Academy of Sciences, Tashkent, Uzbekistan*

^f*INFN Laboratori Nazionali di Frascati, Frascati, Italy*

Abstract

Experimental and theoretical results of the P_{CN} fusion probability of reactants in the entrance channel and the W_{sur} survival probability against fission at deexcitation of the compound nucleus formed in heavy-ion collisions are discussed. The theoretical results for a set of nuclear reactions leading to the formation of compound nuclei (CNs) with the charge number $Z = 102\text{--}122$ reveal a strong sensitivity of P_{CN} to the characteristics of colliding nuclei in the entrance channel, dynamics of the reaction mechanism, and excitation energy of the system. We discuss the validity of assumptions and procedures for analysis of experimental data, and also the limits of validity of theoretical results obtained by the use of phenomenological models. The comparison of results obtained in many investigated reactions reveals serious limits of validity of the data analysis and calculation procedures.

Keywords: Nuclear reactions, fusion probability, surviving probability of CN, heavy and superheavy elements

1. Introduction

The study of the nuclear reactions in heavy ion collisions continues to excite great interest in the scientific community to better understanding the reaction dynamics from the stage of capture of the projectile by target-nucleus up to the formation of the reaction products. The knowledge about reaction dynamics is important in planning possible experiments suitable to form heavy and superheavy compound nuclei leading to evaporation residues (ERs) and identifiable fragments belonging to the fusion-fission process. It is clear that the differences between the experimental results measured for the same quantities in the same nuclear reactions are explained by the specific conditions present in the overall experimental apparatus and data analysis. The differences between the theoretical results calculated by the different models are related to the assumptions made in the procedures of theoretical calculations and use of simplified phenomenological models unsuitable to describe the reaction dynamics. In fact, in this last case the use of free parameters can lead to an apparent acceptable agreement between the calculated results and data but actually these results can not prove the effectiveness of the procedures used to obtain the experimental results. Analogously, the procedure of obtaining the best values of free parameters used in the phenomenological model which leads to results of calculation in good agreement with the obtained experimental results can not demonstrate by a clear and unambiguous way the understanding of the reaction

dynamics, from the stage of colliding nuclei up to the achievement of the final products.

The reliability of the experimental results can be improved by decreasing the number of assumptions due to the increase of the measured physical quantities and their correlation.

The evaporation residues (ERs) are registered enough unambiguously since those products can be separated easily from the ones of the other events. Therefore, theoretical results are aimed to be close to the experimental data of evaporation residues. Furthermore, there are difficulties in estimating the incomplete fusion contribution [1–3] in the formation of the evaporation residues since the ambiguities of its mechanism are appeared.

The main reason for the differences in the experimental fusion and capture cross sections is related to the ambiguity of the procedures at the separation of the events corresponding to deep-inelastic collisions (DICs), quasifission (QF) and fusion-fission (FIS) processes. The quasifission is the decay of the DNS into two fragments without formation of CN. There is still no definite understanding nature of full momentum transfer reactions in the experimental analysis of the deep-inelastic collisions and quasifission events to estimate capture cross sections. The overlap of the mass and/or angular distributions of the quasifission and fusion-fission products causes ambiguity in the estimation of the experimental fusion cross sections.

The choice of degrees of freedom and interaction forces involved in calculations are directed to simplify the complicated or unknown nature of the physical processes of the heavy ion collisions. Therefore, the deviations between the experimental results and the various theoretical ones are inevitable.

Email addresses: ggiardina@unime.it (G. Giardina), gmandaglio@unime.it (G. Mandaglio), nasirov@jinr.ru (A.K. Nasirov)

The P_{CN} fusion probability of reactants in the heavy ion collisions is estimated as a ratio of the complete fusion (σ_{fus}) and capture (σ_{cap}) cross sections:

$$P_{CN} = \frac{\sigma_{fus}}{\sigma_{cap}} = \frac{\sigma_{fus}}{\sigma_{fus} + \sigma_{qfis}}. \quad (1)$$

The capture cross section is determined by the estimation of the range of the orbital angular momentum leading to the full momentum transfer in the entrance channel of collision. The evolution of the excited dinuclear system (DNS) formation can lead to complete fusion in competition with quasifission. The details of this model are present in many of our papers (see, for example, [4–13]), but we give in Appendix A of the paper the main description of the method regarding the reaction in the entrance channel up to the evolution of DNS to complete fusion stage in competition with the decay of DNS into two nuclei by the quasifission process. The model takes into account the dependence of the capture cross section on the range of the orientation angles of nuclei at the initial stage of nuclear collision, the mass asymmetry parameter of reactants in the entrance channel, the considered $E_{c.m.}$ energy range for the investigated reaction, the orbital angular momentum range that are needfull to consider in a refined and sensitive model with the aim of studying the evolution of each reaction from the contact of reactants to the compound nucleus formation, until to obtaining the final products of deexcitation of CN.

It is obvious the differences between the values of P_{CN} extracted from the measured data of the capture and complete fusion events depend on how are correctly estimated capture and fusion cross sections from the measured data. Therefore, the reliable experimental determinations of P_{CN} and consequently the understanding the entrance channel effect on the P_{CN} values are strongly related to the choice of assumptions for the data analysis.

For example, in refs.[4, 14] the ambiguity in the estimation of the experimental quasifission events for the $^{48}\text{Ca} + ^{154}\text{Sm}$ reaction is discussed. The strong difference between the experimental data [15] and theoretical curves of quasifission cross sections in ref. [4] is explained by excluding the quasifission events related to the mass numbers outside the range $60 \leq A \leq 130$ at low energies $E_{c.m.}^* < 140$ MeV. The authors of ref. [15] considered the reaction products with mass numbers $A < 60$ (or $A > 130$) as the ones of the deep-inelastic collisions. The yield of products of the full momentum transfer (capture) reaction is seen from their total kinetic energy distribution presented in ref. [15]. So the reason causing the huge difference between theoretical [4] and experimental [15] results is related to the conditions of determination of the capture events. The separation of the capture events by the restriction of the mass numbers of binary fragments in the range $60 \leq A \leq 130$ is not completely correct since there are events of capture related with yield of binary fragments with mass numbers $A \leq 60$. Such a procedure of restriction at the analysis of the measured data leads to the loss of an unknown part of the capture cross section, and, consequently, the fusion probability P_{CN} obtained by the restriction of the capture events is not realistic. Since a significant part of the quasifission products with the mass numbers $A < 60$ (or

$A > 130$) are excluded from the consideration. Therefore, the reduced capture cross section leads to increase the fusion probability P_{CN} (see Eq. (1)). The presence and overlapping of the quasifission products among DIC products was demonstrated in ref. [14] (see figs. 3 and 4) and ref.[5] (see Fig. 4).

The competition between the complete fusion of nuclei in DNS and quasifission (decay of DNS into two fragments) processes decreases the value of the fusion cross section [16–18]:

$$\sigma_{fus}(E_{c.m.}) = \sum_{\ell=0}^{\ell_d(E_{c.m.})} (2\ell + 1) \sigma_{cap}(E_{c.m.}, \ell) P_{CN}(E_{c.m.}, \ell). \quad (2)$$

The maximum value of ℓ leading to capture $\ell_d(E_{c.m.})$ depends on the beam energy and it is calculated by the solution of the radial motion equations (see ref. [18]). Since the capture cross section is equal to the sum of the complete fusion and quasifission cross sections, $\sigma_{cap} = \sigma_{fus} + \sigma_{qfis}$, the quasifission cross section is calculated by the expression

$$\sigma_{qfis}(E_{c.m.}) = \sum_{\ell=0}^{\ell_d} (2\ell + 1) \sigma_{cap}(E_{c.m.}, \ell) (1 - P_{CN}(E_{c.m.}, \ell)). \quad (3)$$

It should be stressed that quasifission of dinuclear system can take place at all angular momentum values from $\ell = 0$ to ℓ_d . Another binary process which leads to the formation of two fragments similar to those of fusion-fission and quasifission is the fast fission (FF). The fast fission occurs only if there is not a fission barrier for the being formed compound nucleus due to the large values of the angular momentum, $\ell > \ell_f$. According to the rotating liquid drop model (see [19]) a rotating nucleus with the angular momentum ℓ_f breaks down immediately. Therefore, FF is determined as the disintegration of the fast rotating mononucleus into two fragments, though DNS survives quasifission to be transformed into CN. In the case of the superheavy nuclei, the fission barrier providing their stability against fission appears only due to shell effects in their binding energy because there is no barrier connected with the liquid-drop model (see ref.[20]). The damping of the shell effects decreases the possibility of the deformed mononucleus of reaching the CN equilibrium shape, and the mononucleus breaks down into two fragments without to reach the CN stage. Therefore, the fast fission cross section σ_{ff} is calculated by summing the contributions of the partial fusion cross sections with ℓ values corresponding to the range $\ell_f < \ell < \ell_d$ leading to the formation of the mononucleus,

$$\sigma_{ff}(E_{c.m.}) = \sum_{\ell=\ell_f}^{\ell_d} (2\ell + 1) \sigma_{cap}(E_{c.m.}, \ell) P_{CN}(E_{c.m.}, \ell). \quad (4)$$

The sensitivity of the capture σ_{cap} and fusion cross section σ_{fus} to the change of the radius parameter r_0 is discussed in Appendix A of this work. The low energy part of the excitation functions of σ_{cap} and σ_{fus} is moved to lower energies by the increase of the r_0 values. This means that the variation of r_0 from 1.16 fm to 1.18 fm leads to the change of the fusion probability about 2 times at the fixed low value of the beam energy. The part of the excitation functions of σ_{cap} and σ_{fus}

above the Coulomb barrier is less sensitive to the r_0 values. It is clear the change of r_0 leads to an appreciable modification of the interaction barrier of nuclei. This property of the excitation function is used in our calculation to reach an agreement of the capture cross section at the lowest energies with the experimental data. This allows us to use the partial fusion cross sections $\sigma_{\text{cap}}(E_{\text{c.m.}}, \ell)$ to calculate the partial evaporation residues cross sections and the sum them is compared with the experimental data.

As the advantage of our modular system of nuclear reaction codes we stress the possibility to include into calculation explicitly the effect of the orbital angular momentum on the capture, fusion and survival probability. This fact allows us to analyze the role of the entrance channel effects on the evaporation residue cross section [10].

2. About the P_{CN} determination for the CN formation

In Fig. 3 of the ref. [21], the author presents some values of the P_{CN} fusion probability extracted from the experimental data [22, 23] in nuclear reactions leading to CNs with $Z_{\text{CN}}=108$, 112, 114, and 116, and compares them with the trends of some theoretical results presented in refs. [14, 24–26]. These theoretical results are different since they are obtained by different models and computational procedures. Therefore, the comparison between the experimental results and the various theoretical results seems to be formal and does not allow to make analysis of the reasons causing the observed behavior of the fusion probability, though in some cases the theoretical results are substantially consistent with those presented in Fig. 3 of ref. [21]. In order to hold a larger and more general discussion we present in Fig. 1 of the present paper the results of P_{CN} as a function of Z_{CN} for reactions leading to CNs included in the range 102–122 of atomic number of superheavy nuclei (SHN). It is an extension of results presented in Fig. 3 of paper [21] and covering various kinds of reactions from very asymmetric to almost symmetric reactions characterized by the mass asymmetry parameter $\eta = \frac{|A_2 - A_1|}{A_1 + A_2}$. Moreover, in Table 1 there are included all the specific details used to estimate P_{CN} for the reactions leading to the formation of CNs with the charge number Z_{CN} and excitation energy E_{CN}^* which was considered by authors of the corresponding papers. From a whole view of Fig.1 (a), it appears that the experimental data of P_{CN} are underestimated by the theoretical approaches for the same reactions and at the extracting results from the measured data. Such systematic difference between the experimental and theoretical values of the P_{CN} is the evidence of the missing contribution of the quasifission process producing the projectile-like and target-like reaction products or/and considering the quasifission products with mass numbers around the symmetrical mass fragments as ones of the fusion-fission process. Unfortunately, the mass symmetric contributions cannot be quantified and separated from the one resulting from the pure contribution deriving from the fusion-fission process.

To understand the underestimation of the experimental results for P_{CN} by the theoretical calculations it is necessary to

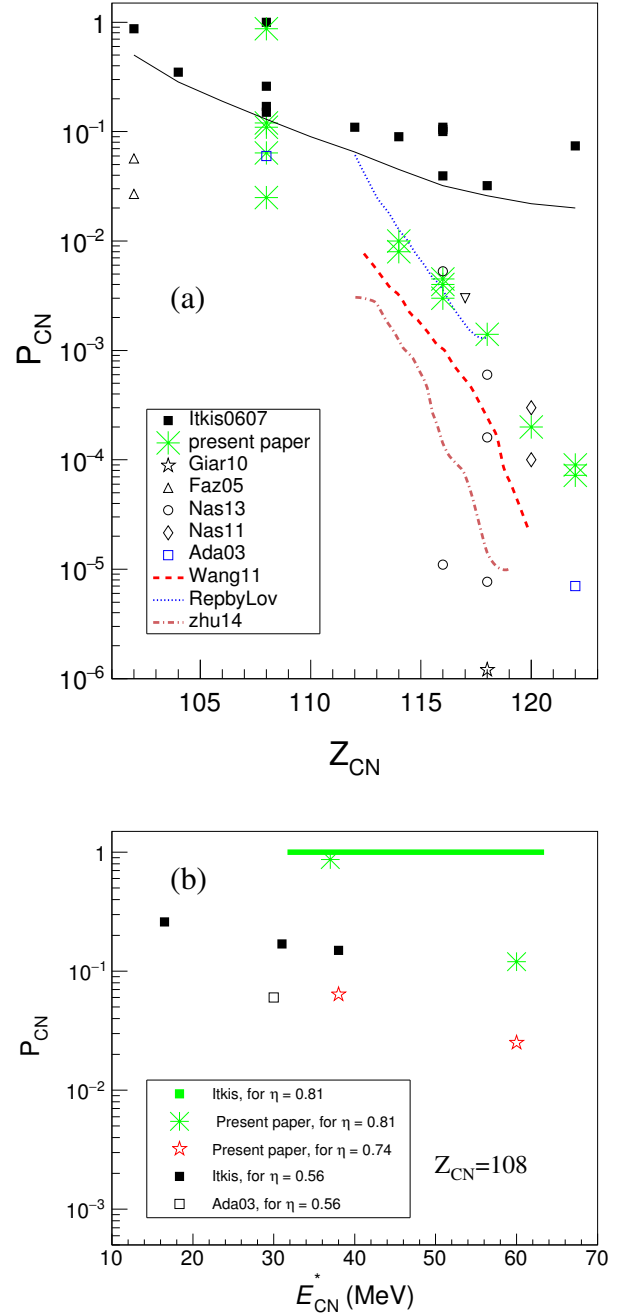


Figure 1: (Color on-line) Comparison of P_{CN} values for many asymmetric, less asymmetric, and almost asymmetric reactions leading to compound nuclei with the atomic numbers Z_{CN} included in the 102–122 range. (a) The P_{CN} experimental values from refs. [22, 23] (full squares), the theoretical values of the present paper (asterisks); the results presented in refs. [5] (open triangles), [6] (open star), [7] (open diamonds), [8] (open circles), [24] (open square), [4] (open inverse triangle), [21, 24] (dotted line), [21, 25] (dashed line), [21, 26] (dash-dotted line); the thin full line is a guide for the eye indicating a clear separation between the experimental P_{CN} determinations and the theoretical P_{CN} values for the investigated reactions. (b) The P_{CN} values vs E_{CN}^* for the set of entrance channel reactions leading to CNs with $Z_{\text{CN}} = 108$ and different mass asymmetry parameters of CN: $^{26}\text{Mg}+^{248}\text{Cm}$ reaction with $\eta = 0.81$, $^{32}\text{S}+^{238}\text{U}$ with $\eta = 0.74$ and $^{58}\text{Fe}+^{208}\text{Pb}$ with $\eta = 0.56$.

make the following remarks and comments on the results presented in Fig. 1 and Table 1, reviewing the various reactions.

2.1. Comparison of P_{CN} results for reactions forming CNs in the $Z_{CN}=102-122$ range

A detailed comparison and analysis between P_{CN} experimental determinations and the related theoretical results is needed in order to understand the reasons of some relevant discrepancies.

1. For the $^{48}\text{Ca}+^{208}\text{Pb}$ reaction leading to the $^{256}_{102}\text{No}$ CN the value of the fusion probability $P_{CN}=0.87$ has been extracted at E_{CN}^* of about 30 MeV from the experimental data of the capture and fusion cross sections in refs. [22, 23] while the theoretical value $P_{CN}=0.027$ has been found in ref. [5] at the excitation energy $E_{CN}^*=30$ MeV (see Fig. 1(a)). There are two reasons causing this large discrepancy between theoretical and experimental results for P_{CN} . **a)** At the extraction of P_{CN} values from the experimental data the contribution of the quasifission events into capture cross section with the mass numbers around $A=50$ has been neglected although those events are the full momentum transfer events [27–29]. This means that the quasifission events with the mass numbers around initial mass numbers $A=50$ considered as deep-inelastic collisions and the quasifission cross section σ_{qfs} is underestimated of one order of magnitude in calculations of P_{CN} by experimentalists. As a result the value of P_{CN} increased (see Fig. 2 of ref. [5]). **b)** On the other hand, due to the inclusion of the quasifission and fast fission events occurring at large values of the orbital angular momentum of collision into the fusion-fission events, the experimental fusion cross section σ_{fus} was overestimated. As a result, the experimental value of P_{CN} appears larger. It is well known that the fast fission products are mixed with the fusion-fission ones and it is impossible to separate the contributions between these two processes. This circumstance leads to an increase of the fusion cross section σ_{fus} . Obviously these two defects of the procedure at the analysis of the experimental data increase the P_{CN} value. The similar difference is seen from the comparison of the experimental and theoretical results of the P_{CN} values 0.35 from [22, 23] and 0.027 from [5], respectively, for two close mass asymmetric reactions ($\eta = 0.63$ and 0.61, respectively) $^{50}\text{Ti}+^{208}\text{Pb}$ and $^{48}\text{Ca}+^{208}\text{Pb}$ at the same excitation energy $E_{CN}^* = 30$ MeV.
2. In Fig. 1 (b) the P_{CN} values vs E_{CN}^* for the reactions with different mass asymmetry parameters $\eta = |A_1 - A_2|/(A_1 + A_2)$ leading to CNs with $Z_{CN} = 108$ demonstrate the role of the entrance channel: thick line represents the experimental determinations $P_{CN} = 1$ given in [22, 23] for the very asymmetric reaction $^{26}\text{Mg}+^{248}\text{Cm}$ ($\eta=0.81$) leading to $^{274}108$ CN; in this figure, asterisks represent the theoretical values of P_{CN} for the same reaction found in the present paper; open stars represent the P_{CN} theoretical values obtained in the present paper for the less asymmetric reaction $^{36}\text{S}+^{238}\text{U}$ ($\eta = 0.74$) leading to the

same $^{274}108$ CN. In the same figure full and open squares represent the experimental [22, 23] and theoretical value [24] obtained for the $^{58}\text{Fe}+^{208}\text{Pb}$ reaction. It is seen that the experimental data are about 3 times higher than the theoretical ones. It can be concluded that: i) the dependence of the experimental values of P_{CN} [22, 23] are less sensitive to E_{CN}^* than the one of its theoretical values: P_{CN} value for the $^{26}\text{Mg}+^{238}\text{U}$ reaction decreases by more than 7 times at the increase of the E_{CN}^* excitation energy from 37 to 60 MeV; ii) similarly, our theoretical P_{CN} values for the $^{36}\text{S}+^{238}\text{U}$ less asymmetric reaction ($\eta = 0.74$) decrease with increasing the E_{CN}^* values; iii) the P_{CN} values for a less asymmetric reaction are smaller than the ones for a more asymmetric reaction; iv) the experimental P_{CN} result extracted at $E_{CN}^* = 31$ MeV by using the capture and fusion cross sections reported in refs. [22, 23] for the $^{58}\text{Fe}+^{208}\text{Pb}$ reaction leading to $^{266}108$ CN with mass asymmetry parameter $\eta = 0.56$ is about three times higher than the value found in ref. [24] at the comparable excitation energy of $E_{CN}^* = 30$ MeV; moreover, we have to observe that in Table 1 the $P_{CN} = 0.064$ value found in the present paper for the more asymmetric $^{36}\text{S}+^{238}\text{U}$ reaction with mass asymmetry parameter $\eta = 0.74$ leading to the same element with $Z_{CN}=108$ and mass number $A=274$ at excitation energy $E_{CN}^* = 38$ MeV is consistent with the $P_{CN} = 0.06$ value found in [24]. These results clearly demonstrate the great sensitivity of the P_{CN} function to the E_{CN}^* excitation energy of CN for each considered entrance channel reaction. It is well known that the P_{CN} value is smaller for a less asymmetric reaction (and a fortiori for the less asymmetric reaction as for example the considered $^{58}\text{Fe}+^{208}\text{Pb}$) than the one obtained for a very asymmetric reaction at a given E_{CN}^* excitation energy of CN. This phenomenon is related to the landscape of driving potential where the two different entrance channels has different initial conditions to reach the same CN. The different properties of the CN formation are caused by the different values of the intrinsic fusion B_{fus}^* and quasifission B_{qf} barriers for the two mass asymmetry parameters characterizing the entrance channels (see for example [7, 8, 10]).

The increased sensitivity of the change of P_{CN} obtained in theoretical estimations to the mass asymmetry in the entrance channel allows us to separate the quasifission products from the ones of the fusion-fission process contributing to the total fragment formation, while this cannot be unambiguously experimentally verified [4, 27–30]. Since the products of the quasifission process are strongly prominent with respect to the ones of the fusion-fission process when comparing fragments produced by symmetric (or almost symmetric) reactions with those produced by asymmetric reactions, the correct analysis of the mass, energy and angular distribution of the reaction fragments allows us to establish process producing them to a reliable description of the reaction dynamics.

3. The fusion probabilities determined from the experimental capture and fusion excitation functions of the $^{48}\text{Ca}+^{238}\text{U}$

Table 1: Measured and calculated P_{CN} fusion probabilities obtained at E_{CN}^* excitation energies for the listed reactions with mass asymmetric parameter $\eta = \frac{|A_2 - A_1|}{A_1 + A_2}$ leading to CNs with atomic numbers Z_{CN} included in the $Z_{CN}=102-122$ range. The presented P_{CN} experimental values range between 1 and 3.2×10^{-2} for the excitation energy values of CN included in the 16.5–63.4 MeV interval, whereas our calculated P_{CN} values range between 0.87 and 7.7×10^{-6} for the corresponding excitation energy values of CN included in 16–60 MeV interval.

Reaction	η	Z_{CN}	CN	Measured P_{CN}	Calculated P_{CN}	E_{CN}^* (MeV)	reference
$^{48}\text{Ca}+^{208}\text{Pb}$	0.63	102	256	0.87		~30	[22, 23]
$^{48}\text{Ca}+^{208}\text{Pb}$	0.63	102	256		0.027	30	[5]
$^{48}\text{Ca}+^{208}\text{Pb}$	0.63	102	256		0.057	16	[5]
$^{50}\text{Ti}+^{208}\text{Pb}$	0.61	104	258	0.35		~30	[22, 23]
$^{58}\text{Fe}+^{208}\text{Pb}$	0.56	108	266	0.26		16.5	[22, 23]
$^{58}\text{Fe}+^{208}\text{Pb}$	0.56	108	266	0.17		31	[22, 23]
$^{58}\text{Fe}+^{208}\text{Pb}$	0.56	108	266	0.15		38	[22, 23]
$^{58}\text{Fe}+^{208}\text{Pb}$	0.56	108	266		0.06	30	[24]
$^{36}\text{S}+^{238}\text{U}$	0.74	108	274		0.064	38	present paper
$^{36}\text{S}+^{238}\text{U}$	0.74	108	274		0.025	60	present paper
$^{26}\text{Mg}+^{248}\text{Cm}$	0.81	108	274	1		from 31.7 to 63.4	[22, 23]
$^{26}\text{Mg}+^{248}\text{Cm}$	0.81	108	274		0.87	37	present paper
$^{26}\text{Mg}+^{248}\text{Cm}$	0.81	108	274		0.12	60	present paper
$^{48}\text{Ca}+^{238}\text{U}$	0.664	112	286	0.11		32	[22, 23]
$^{48}\text{Ca}+^{244}\text{Pu}$	0.67	114	292	0.08		32	[22, 23]
$^{48}\text{Ca}+^{244}\text{Pu}$	0.67	114	292		0.008	32	present paper
$^{48}\text{Ca}+^{244}\text{Pu}$	0.67	114	292		0.01	37	present paper
$^{48}\text{Ca}+^{246}\text{Cm}$	0.674	116	294	0.11		32.5	[22, 23]
$^{48}\text{Ca}+^{248}\text{Cm}$	0.676	116	296	0.047		32	[22, 23]
$^{48}\text{Ca}+^{248}\text{Cm}$	0.676	116	296		5.3×10^{-3}	33	[8]
$^{48}\text{Ca}+^{248}\text{Cm}$	0.676	116	296		0.004	37	present paper
$^{50}\text{Ti}+^{244}\text{Pu}$	0.66	116	294	0.105		41.5	[22, 23]
$^{50}\text{Ti}+^{244}\text{Pu}$	0.66	116	294	0.10		51.5	[22, 23]
$^{50}\text{Ti}+^{244}\text{Pu}$	0.66	116	294		0.003	35	present paper
$^{50}\text{Ti}+^{244}\text{Pu}$	0.66	116	294		0.0045	41	present paper
$^{58}\text{Fe}+^{232}\text{Th}$	0.60	116	290		1.1×10^{-5}	40	[8]
$^{48}\text{Ca}+^{249}\text{Bk}$	0.68	117	297		3×10^{-3}	33	[4]
$^{48}\text{Ca}+^{249}\text{Cf}$	0.68	118	297		0.6×10^{-3}	33	[6, 8]
$^{48}\text{Ca}+^{249}\text{Cf}$	0.68	118	297		0.14×10^{-2}	37	present paper
$^{64}\text{Ni}+^{232}\text{Th}$	0.57	118	296		7.7×10^{-6}	35	[8]
$^{64}\text{Ni}+^{232}\text{Th}$	0.57	118	296		1.6×10^{-4}	40	[8]
$^{86}\text{Kr}+^{208}\text{Pb}$	0.42	118	294	0.032		~30	[22, 23]
$^{86}\text{Kr}+^{208}\text{Pb}$	0.42	118	294		2×10^{-5}	30	[6]
$^{50}\text{Ti}+^{249}\text{Cf}$	0.666	120	299		3×10^{-4}	33	[7]
$^{54}\text{Cr}+^{248}\text{Cm}$	0.64	120	302		1×10^{-5}	30	[7]
$^{54}\text{Cr}+^{248}\text{Cm}$	0.64	120	302		2×10^{-4}	37	present paper
$^{58}\text{Fe}+^{248}\text{Cm}$	0.63	122	306	0.07		33	[22, 23]
$^{58}\text{Fe}+^{248}\text{Cm}$	0.63	122	306		7×10^{-6}	33	[24]
$^{54}\text{Cr}+^{249}\text{Cf}$	0.644	122	303		7.2×10^{-5}	33	present paper
$^{54}\text{Cr}+^{249}\text{Cf}$	0.644	122	303		9×10^{-5}	37	present paper

and $^{48}\text{Ca}+^{244}\text{Pu}$ reactions leading to the different $^{286}112$ and $^{292}114$ CNs, respectively, presented in refs. [22, 23] at $E_{\text{CN}}^*=32$ MeV are very close like $P_{\text{CN}}=0.11$ and 0.08 (see Table 1), respectively, whereas in our theoretical study on the $^{48}\text{Ca}+^{244}\text{Pu}$ reaction in the present work we find the value $P_{\text{CN}}=0.008$ for the fusion probability at $E_{\text{CN}}^*=32$ MeV (see Table 1) that is 1 order of magnitude smaller than the one found in [22, 23]. The reason of this relevant difference is related with procedures at extraction of the experimental values of the P_{CN} by restriction of the mass and angular distributions of the binary reaction products to determine ones related with quasifission process.

4. By considering the group of reactions leading to isotopes of the $Z_{\text{CN}} = 116$ element, one needs to make the following comments: the results of the P_{CN} extracted from the measured data [22, 23] show that the values for the $^{48}\text{Ca}+^{246}\text{Cm}$ and $^{48}\text{Ca}+^{248}\text{Cm}$ reactions are 0.11 (at $E_{\text{CN}}^*=32.5$ MeV) and 0.05 (at $E_{\text{CN}}^*=32$ MeV), respectively, whereas our calculations [8] give values $P_{\text{CN}}=5.3\times 10^{-3}$ at $E_{\text{CN}}^*=33$ MeV for the $^{48}\text{Ca}+^{248}\text{Cm}$ reaction (1 order of magnitude smaller than the experimental determination at about the same E_{CN}^*), and $P_{\text{CN}} = 1.1 \times 10^{-5}$ (at $E_{\text{CN}}^*=40$ MeV) for the $^{58}\text{Fe}+^{232}\text{Th}$ reaction (see Table 1). Therefore, our theoretical results of P_{CN} are strongly sensitive to the entrance channel reaction and excitation energy (see Table 1), whereas, the experimental determinations of P_{CN} appear essentially insensitive to the above-mentioned reactions and excitation energy (see Table 1). In fact, in all these cases the experimental values appear almost insensitive to the various entrance channels and values of the E_{CN}^* excitation energy; therefore, also these experimental results are very different from our calculated values. Moreover, the measurements [22, 23] on the $^{50}\text{Ti}+^{244}\text{Pu}$ reaction give the same values as $P_{\text{CN}}=0.1$ at both $E_{\text{CN}}^*=41.5$ and 51.5 MeV excitation energies, instead we find the value 4.5×10^{-3} at $E_{\text{CN}}^*=41$ MeV that is over 20 times smaller than the measured one.
5. For the $^{48}\text{Ca}+^{249}\text{Bk}$ reaction ($\text{CN}=^{297}117$) we obtained [4] $P_{\text{CN}}=3\times 10^{-3}$ at $E_{\text{CN}}^*=33$ MeV. The values of P_{CN} found for the close $^{48}\text{Ca}+^{248}\text{Cm}$ and $^{48}\text{Ca}+^{249}\text{Cf}$ reactions leading to the $^{296}116$ and $^{297}118$ CNs, respectively, are equal to 5.3×10^{-3} and 6×10^{-4} (see Table 1), respectively, at $E_{\text{CN}}^*=33$ MeV. These results demonstrate the sensitivity of the P_{CN} value with the entrance channel and at the same time the consistency with reliable results. In the reaction induced by the ^{48}Ca beam and different targets like ^{248}Cm , ^{249}Bk , and ^{249}Cf with $Z_{\text{CN}}=96, 97, 98$, respectively, the P_{CN} values appreciably decrease (see Table 1) due to the increase of the Coulomb potential.
6. For the reaction leading to compound nucleus with $Z_{\text{CN}} = 118$ we can compare the experimental and theoretical P_{CN} values. The $P_{\text{CN}}=0.032$ value (at $E_{\text{CN}}^*=30$ MeV) experimentally found in [22, 23] for the $^{86}\text{Kr}+^{208}\text{Pb}$ reaction is three orders of magnitude greater than the theoretical estimation $P_{\text{CN}}=2\times 10^{-5}$ (at $E_{\text{CN}}^*=30$ MeV) presented by us in [6]. Analogously, the measured value $P_{\text{CN}}=0.07$ at $E_{\text{CN}}^*=33$ MeV obtained in the experiment [22, 23] with

the $^{58}\text{Fe}+^{248}\text{Cm}$ reaction leading to the $^{306}122$ CN is four orders of magnitude greater than the theoretical value $P_{\text{CN}} = 7 \times 10^{-6}$ at $E_{\text{CN}}^*=33$ MeV obtained in [24]. Therefore, even in these cases of the less mass asymmetric reactions leading to superheavy CNs it is possible to observe unreliable results of P_{CN} deduced by the analysis of the experimental data.

In conclusion, a large part of our P_{CN} theoretical results reported in Fig. 1 is in agreement with the results obtained in [24] and for some reactions our results are consistent with the ones obtained in [25, 26]. Apart from some differences in P_{CN} values obtained with different theoretical models, it is relevant the common sensitivity of the theoretical results as a function of the mass asymmetry parameter, excitation energy E_{CN}^* , and the Z_{CN} atomic number of the CN reached. Conversely, the P_{CN} results as a function of Z_{CN} obtained from the analysis of the experimental data given in [22, 23] are larger in comparison with our theoretical results and those obtained by other models (see Fig. 1), where the experimental P_{CN} values range between 1 and 3.2×10^{-2} in the $\Delta E_{\text{CN}}^* = 16.5-63.4$ MeV interval, whereas our calculated P_{CN} values range between 0.87 and 7.7×10^{-6} for the comparable excitation energy range of CNs included in the 16–60 MeV interval. The results presented in Fig 1 and Table 1 for all reactions leading to compound nuclei included in $Z_{\text{CN}}=102-122$ interval of atomic number clearly demonstrate that the P_{CN} experimental determinations appear to be poorly sensitive to the mass asymmetry parameter η of the entrance channel and also to the excitation energy E_{CN}^* value. Such a large general difference between the P_{CN} experimental determinations and the corresponding theoretical values, for a wide set of investigated reactions leading to heavy and superheavy compound nuclei, is the clear evidence of the unreliable experimental estimation of the contribute due to the quasifission process during the evolution of the capture events into compound nucleus formation. In fact, as already explained, there is in experimental analysis some ambiguity in the separation of the capture events from the huge contribution coming from the deep-inelastic collisions; therefore, the adopted assumptions in the data analysis lead to a relevant uncertainty in the capture cross section determination. Moreover, for the experimental determination of the compound nucleus cross section it is necessary to made some assumption for the mass of the detected fragments which contribute to the true fusion-fission process. Even for this experimental determination, the constraint used in the analysis to select the events with symmetric mass only do not overcome the problem of the correct determination of the fusion cross section because in the reactions considered in Fig 1 and Table 1, the mass symmetric distribution contributed by the quasifission and fast-fission processes are very relevant. Therefore, the experimental determination of the capture and fusion cross section are affected by strong uncertainties, and consequently the experimental P_{CN} ratio determinations between the capture and fusion cross sections are unreliable.

2.2. Discussion on the P_{CN} results

The reason for this discrepancy between the measured data and theoretical values of P_{CN} is connected with the experimental difficulties in the identification of the fusion-fission fragments produced by fission of the compound nucleus to determine the fusion cross section. The mass distribution of the fast fission and sometimes quasifission processes overlaps with the mass symmetrical fusion-fission product distributions. The ability of the correct extraction of the fusion-fission cross section from the mixed data of the reaction products decreases due to intensive population of the mass-symmetric region by the fast fission or/and the quasifission fragments by the increase of E_{CN}^* . Therefore, the extraction of the fusion cross section from the experimental data is strongly affected by the underestimation of contribution of the fast fission and quasifission fragments. This problem is inherent to all kinds of reactions, leading to the formation of superheavy nuclei, when experimentalists selecting only mass symmetric fragments with the mass numbers in the range $A_{CN}/2 \pm 20$, assume such products belong only to the fusion-fission process. In fact, this assumption is completely doubtful because the yield of mass symmetric fragments produced by the quasifission and fast fission processes are competitive and often some orders of magnitude higher than the ones produced by the fusion-fission process (see for example, refs. [16, 31]).

The estimate of the capture cross section is affected by relevant uncertainty in the separation of capture events of projectile by the target nucleus from the deep inelastic collisions with high yield. The missing the quasifission events at the restriction of the mass distribution of the binary products also leads to increase the experimental P_{CN} values. Therefore, the experimental estimate of the P_{CN} fusion probability by the $\sigma_{fus}/\sigma_{cap}$ ratio (where the σ_{fus} and σ_{cap} values are determined in experiments with large uncertainty) is also affected by great uncertainty by a factor that changes with E_{CN}^* excitation energy of CN, and with the asymmetry/symmetry of the entrance channel. Of course the P_{CN} value also strongly changes with the mass number A of CN at the same atomic number Z_{CN} , and even at different Z_{CN} (see Fig. 3 of paper [21] and with more details in Fig. 1 of the present paper, especially the set of the reactions leading to CNs with $Z_{CN}=108, 116, 118, \text{ and } 122$).

By regarding Fig. 4 of paper [21] where the measured P_{CN} values of ref. [15] are compared with the predicted P_{CN} values of ref. [32] against the E_{CN}^* excitation energy of CN. The author used there P_{CN} values from the paper [14] presented against the collision energy relative to the interaction barriers $E_{c.m.} - E_B$. Unfortunately the author [21] has not performed appropriately transformation of the E_{CN}^* excitation energy from the $E_{c.m.} - E_B$ values: the position of the dashed curve from [14] is moved on 15 MeV to higher energy. Why? We add in Fig. 2 of the present paper our calculated P_{CN} values for the $^{16}\text{O}+^{186}\text{W}$ very asymmetric reaction and for the less asymmetric $^{48}\text{Ca}+^{154}\text{Sm}$ reaction, also including for a comparison the sets of P_{CN} values cited in paper [21] as the measured values of ref.[15] and the predicted values of ref.[32]. As Fig. 2 shows the experimental P_{CN} values for the $^{48}\text{Ca}+^{154}\text{Sm}$ strongly increase with the increase of the E_{CN}^* excitation energy of the ^{202}Pb CN from 0.33

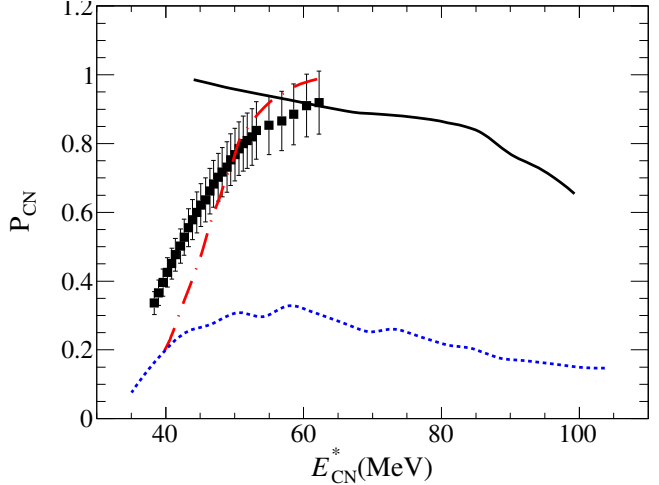


Figure 2: (Color on-line) The P_{CN} fusion probability as a function of the E_{CN}^* excitation energy for the $^{16}\text{O}+^{186}\text{W}$ very asymmetric reaction and for the $^{48}\text{Ca}+^{154}\text{Sm}$ less asymmetric reaction presented in [14] (full and dotted lines, respectively). Full squares are the experimental determinations by ref. [15] for the $^{48}\text{Ca}+^{154}\text{Sm}$ reaction and dash-dotted line represents the predicted P_{CN} values for the same reaction by authors of ref. [32].

at $E_{CN}^* = 38$ MeV to 0.93 at $E_{CN}^* = 62$ MeV in about 24 MeV of the ΔE_{CN}^* energy interval. Instead, the theoretical results of P_{CN} presented in Fig. 2, obtained by us for the $^{16}\text{O}+^{186}\text{W}$ and $^{48}\text{Ca}+^{154}\text{Sm}$ very asymmetric and less asymmetric reactions, respectively, show complete different trends for shape and values. At $E_{CN}^* = 35$ MeV P_{CN} is 0.075 for the reaction induced by ^{48}Ca , while at $E_{CN}^* = 44$ MeV the P_{CN} is 1 for the asymmetric reaction induced by ^{16}O , both leading to the same ^{202}Pb CN. Moreover, at $E_{CN}^* = 62$ MeV the P_{CN} value calculated by us for the asymmetric ^{16}O induced reaction is about 0.91 and decreases with the increase of E_{CN}^* , while the P_{CN} calculated by authors [32] is 0.99 for the less asymmetric reaction induced by ^{48}Ca (see dash-dotted line in Fig. 2).

The trend of the P_{CN} values presented by us for the two above-mentioned reactions (full and short-dashed lines) shows the specific sensitivity of the reaction mechanism for the two different entrance channels; instead, the trend of results (full squares and dash-dotted line) presented by authors in papers [15] and [32] for the $^{48}\text{Ca}+^{154}\text{Sm}$ reaction appears fully inconsistent with our sensitive results and therefore they are very questionable. Moreover, in order to show the sensitivity of the P_{CN} with the angular momentum ℓ at two different excitation energies of 49 and 63 MeV (dotted and full lines, respectively) of the formed ^{202}Pb compound nucleus, we present in Fig. 3 our results obtained for the $^{48}\text{Ca}+^{154}\text{Sm}$ less asymmetric reaction. We also present in the same figure the P_{CN} values vs ℓ obtained for the $^{16}\text{O}+^{186}\text{W}$ very asymmetric reaction, leading to the same ^{202}Pb CN at $E_{CN}^*=63$ MeV (dashed line). This figure clearly shows the strong dependence of the P_{CN} results on the excitation energy E_{CN}^* and/or of the beam-target combination in the entrance channel.

Therefore, the comparison of the P_{CN} values for different conditions of reactions can be made and understood only if somebody is able to explain the reasons for different results and

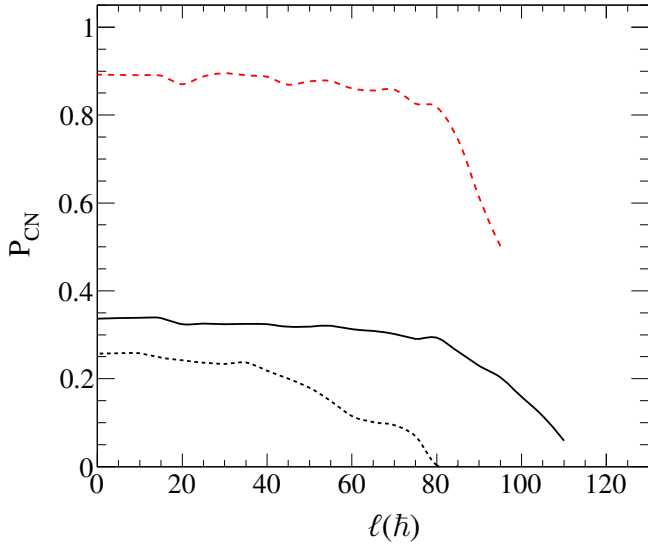


Figure 3: (Color on-line) The P_{CN} fusion probability as a function of the angular momentum ℓ for the $^{16}\text{O}+^{186}\text{W}$ very asymmetric reaction at excitation energy $E_{\text{CN}}^*=75$ MeV (dashed line) of the ^{202}Pb CN is shown; in the same figure, the P_{CN} values vs ℓ for the $^{48}\text{Ca}+^{154}\text{Sm}$ less asymmetric reaction at excitation energies $E_{\text{CN}}^*=49$ and 63 MeV, respectively (dotted and full lines), are also reported.

trend due to the entrance channel effects and/or characteristics of the reaction mechanism.

There is an alternative way of the estimation of the fusion probability by the use of the solution of the master equation (A.9). Y_Z characterizes the population of the DNS configuration with the charge asymmetry $Z = Z_1$ ($Z_2 = Z_P + Z_T - Z$). The initial conditions are $Y_Z(0) = 1$ for $Z = Z_P$ and $Z_2 = Z_T$, where Z_P and Z_T are the charge numbers of the colliding nuclei. The fusion probability is found by calculation of the total quasifission probability P_{qf} from all charge configuration of DNS. The last quantity is calculated by summation of the all decays from the DNS configuration Z :

$$P_{\text{CN}}(t) = 1 - P_{qf}(t), \quad (5)$$

$$P_{qf}(t) = \sum_Z \int_0^t \Lambda_Z^{qf} Y_Z(t') dt'. \quad (6)$$

Its dependence on time calculated for the $^{48}\text{Ca}+^{154}\text{Sm}$ reaction at the excitation energy $E_{\text{CN}}^* = 49$ MeV is presented in Fig. 4. Its asymptotic value is close to the values of P_{CN} calculated by the branching ratio (A.16) of the level densities. Our experience shows that the method of calculation presented in Section Appendix A allows us to include the peculiarities of the driving potential and dependence on the angular momentum of the DNS more evidently. As a result the effects of the entrance channel on the fusion probability appear more precisely.

3. About the W_{sur} survival probability and ER residual nuclei formation

Another important problem in the analysis of the experimental data is related with the determination of the reliable B_{fis}

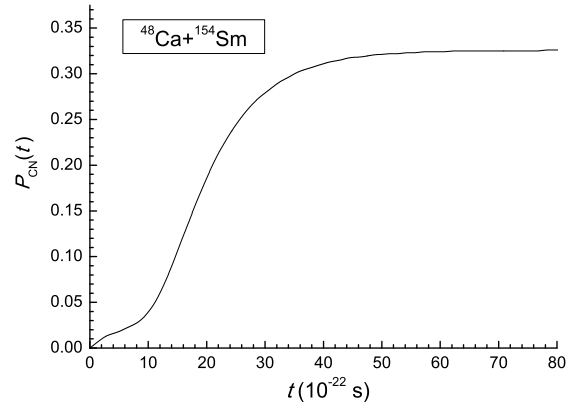


Figure 4: The $P_{\text{CN}}(t)$ fusion probability calculated by Eq.(5) as a function of time for the $^{48}\text{Ca}+^{154}\text{Sm}$ at excitation energy $E_{\text{CN}}^*=49$ MeV and $\ell=20$ \hbar .

fission barrier values of excited nuclei reached along the deexcitation cascade of CN in order to correctly estimate the overall $W_{\text{sur}}(E_{\text{CN}}^*)$ survival probability against fission which is used to calculate the total ER cross section vs E_{CN}^* . Indeed, the experimental determinations of the ERs values may be uncertain whether any of α -decay lifetime of reached nuclei along the deexcitation cascade is less than few μs . The uncertainty in determination of the ERs values appears even more strongly when the process of the deexcitation of CN by the evaporation of the charged particles is neglected in comparison with the evaporation of neutral particles. In fact, in many heavy-ion reactions leading to formation of the heavy and superheavy compound nuclei, the total evaporation residue cross sections (when the charged particles are taken into account too) are much higher than the ones obtained for the evaporation of neutrons only. For example, the $\sigma_{\text{ERtot}}/\sigma_{\text{ER-xn}}$ ratio is 5–8 times for the $^{26}\text{Mg}+^{248}\text{Cm}$ and $^{36}\text{S}+^{238}\text{U}$ reactions (leading to the same $^{274}108$ CN called $^{274}\text{Hs}^*$) and it can reach even 1 or 2 orders of magnitude for some other reactions (see for example [10, 33]). Therefore, neglecting the contribution of the charged particles in the determination of evaporation residue nuclei without the possibility of knowing the effect on the final results is doubtful. We can conclude here that the complete evaporation residue cross section σ_{ERtot} can be determined correctly if there is a possibility of full detection of all the total evaporation residue nuclei in the reaction.

But, practically, it is impossible to determine experimentally at each step (or even at the first step only) the probability of the deexcitation cascade from a nucleus with excitation energy E^* emitting only ν neutrons. In ref. [21] the author attracts attention on the deduced value $\Gamma_n/\Gamma_{\text{total}} = 0.89 \pm 0.13$ [34] (in the $^{26}\text{Mg}+^{248}\text{Cm}$ reaction) for the first step of the ^{274}Hs CN decay at $E_{\text{CN}}^*=63$ MeV of excitation energy by measurement of the angular distribution of the neutrons associated with the fission fragments in the $^{26}\text{Mg}+^{248}\text{Cm}$ reaction, while in our investigation [13] we obtain the value $\Gamma_n/\Gamma_{\text{total}} = 0.17$ for the same reaction and conditions. The author [21] concludes that a highly excited nucleus decays with the vanishingly small fission probability and emits more faster a neutron rather than fis-

sion. But this statement in [21] is clearly based on the information about the B_{fis} fission barrier of about 11 MeV at $E_{\text{CN}}^* = 63$ MeV as reported in Fig. 4 of [34] for the investigated reaction $^{26}\text{Mg} + ^{248}\text{Cm}$. In fact, the value $B_{\text{fis}} = 11$ MeV is unjustifiable since the macroscopic component of the fission barrier is zero for the ^{274}Hs CN and the microscopic component is 4.37 MeV (shell correction at $\ell=0$ and at ground state) (see ref.[35]); moreover, with the increase of the excitation energy E_{CN}^* and angular momentum ℓ decreases the fission barrier of the ^{274}Hs CN. Therefore, at $E_{\text{CN}}^* = 60$ MeV the effective fission barrier of the ^{274}Hs is lower than 1 MeV. Only assuming the dissipation coefficient $\gamma \approx 18$ [36] it is possible in principle to justify the needed delay of the fission process, but nobody knows what mechanism, excited nuclear structure or large amplitude collective motion could produce such a high viscosity for this ^{274}Hs compound nucleus.

Moreover, it is easy to prove the non physical consequence of the result $\Gamma_n/\Gamma_{\text{tot}} = 0.89$ found [34] at the first step of deexcitation cascade of the ^{274}Hs CN at $E_{\text{CN}}^* = 63$ MeV. In fact, if this is true then the following $^{273}\text{Hs}^*$, $^{272}\text{Hs}^*$... $^{267}\text{Hs}^*$ excited hassium isotopes are reached after neutron emission along the deexcitation cascade of the $^{274}\text{Hs}^*$ CN and their shell corrections will be higher than the one of $^{274}\text{Hs}^*$ (see for example the tables in [35, 37–39]) due to the decrease of damping at the cooling the excited hassium isotopes after neutron emission. This circumstance leads to the conclusion that at each step of the deexcitation cascade of the CN the fission barrier B_{fis} increases and the $\Gamma_n/\Gamma_{\text{tot}}$ ratio for each reached intermediate excited hassium isotopes ($^{273}\text{Hs}^*$, $^{272}\text{Hs}^*$... $^{267}\text{Hs}^*$..) must be larger than the one determined by the authors [34] at the first neutron evaporation of the ^{274}Hs CN. Therefore, since the σ_{fus} fusion cross section at $E_{\text{CN}}^* = 63$ MeV is about $0.12 \times \sigma_{\text{capture}}$ (where the σ_{capture} capture cross section is about 10^3 mb), starting from the $\Gamma_n/\Gamma_{\text{tot}}$ value of 0.9 determined [34] at first step of neutron evaporation of CN, one should find a value of the total ER_{xn} cross section of about 10^{-3} mb, instead the experimental value found for the evaporation residue cross sections in the $^{26}\text{Mg} + ^{248}\text{Cm}$ reaction is some picobarn [40]. In fact, we find for the $\Gamma_n/\Gamma_{\text{tot}}$ ratio the value of 0.17 [13] at first step of neutron evaporation from the ^{274}Hs CN at $E^* = 63$ MeV; this value is consistent with the other following $\Gamma_n/\Gamma_{\text{tot}}$ ratios along the deexcitation cascade of the compound nucleus (see Fig. 10 of paper [13]). Therefore, our present value of $W_{\text{sur}} = 6 \times 10^{-14}$ for the complete survival probability is consistent with the measured [40] total ER cross section of some pb after neutron emission only. Consequently, the P_{CN} fusion probability vs E_{CN}^* found in [22, 23] for the $^{26}\text{Mg} + ^{248}\text{Cm}$ reaction, and the W_{sur} survival probability found by [34] at the first neutron emission from the ^{274}Hs CN with $E^* = 63$ MeV of excitation energy are clearly inconsistent because the combination of these results at first step of deexcitation cascade with the following steps of the deexcitation can not be in agreement with the experimental determination [40] of the total ER_{xn} cross section of about 1 pb.

The evaporation residue cross sections at the given values of the CN excitation energy E_x^* at each step x of the deexcitation

cascade by the advanced statistical model [12]

$$\sigma_{\text{ER}}^{(x)}(E_x^*) = \sum_{\ell=0}^{\ell_d} (2\ell + 1) \sigma_{\text{ER}}^{(x)}(E_x^*, \ell), \quad (7)$$

where $\sigma_{\text{ER}}^{(x)}(E_x^*, \ell)$ is the partial cross section of ER formation obtained after the emission of particles $\nu(x)n + y(x)p + k(x)\alpha + s(x)$ (where $\nu(x)$, y , k , and s are numbers of neutrons, protons, α -particles, and γ -quanta) from the intermediate nucleus with excitation energy E_x^* at each step x of the deexcitation cascade by the formula (for more details, see papers [5, 12, 17]):

$$\sigma_{\text{ER}}^{(x)}(E_x^*, \ell) = \sigma_{\text{ER}}^{(x-1)}(E_{x-1}^*, \ell) W_{\text{sur}}^{(x)}(E_{x-1}^*, \ell). \quad (8)$$

At $x = 1$ we deal with the partial fusion cross section: $\sigma_{\text{ER}}^{(0)}(E_0^*, \ell) = \sigma_{\text{fus}}(E_{\text{CN}}^*, \ell)$. In Eq. (8), $\sigma_{\text{ER}}^{(x-1)}(E_{x-1}^*, \ell)$ is the partial cross section of the intermediate excited nucleus formation at the $(x - 1)$ th step, and $W_{\text{sur}}^{(x)}$ is the survival probability of the x th intermediate nucleus against fission along all steps of the deexcitation cascade of the CN.

In calculation of the $W_{\text{sur}}^{(x)}(E_{x-1}^*, \ell)$ the fission barrier is used as a sum of the parametrized macroscopic fission barrier $B_{\text{fis}}^m(\ell)$ depending on the angular momentum ℓ [19] and the microscopic (shell) correction $\delta W = \delta W_{\text{sad}} - \delta W_{\text{gs}}$ due to shell effects; by considering the large deformation of a fissioning nucleus at the saddle point, δW_{sad} is much smaller than the δW_{gs} value and the microscopic shell correction δW to the fission barrier can be expressed by the relation $\delta W \cong -\delta W_{\text{gs}}$. Therefore, an effective fission barrier, as a function of ℓ and T for each excited nucleus formed at various steps along the deexcitation cascade of CN, is calculated by the expression

$$B_{\text{fis}}(\ell, T) = c B_{\text{fis}}^m(\ell) - h(T) q(\ell) \delta W, \quad (9)$$

where the factor c was set to 1 in all our calculations and $h(T)$ and $q(\ell)$ represent the damping functions of the nuclear shell correction (usually it is $\delta W < 0$) with the increase of the excitation energy E^* and ℓ angular momentum, respectively [12]:

$$h(T) = \{1 + \exp[(T - T_0)/d]\}^{-1} \quad (10)$$

and

$$q(\ell) = \{1 + \exp[(\ell - \ell_{1/2})/\Delta\ell]\}^{-1}, \quad (11)$$

where, in Eq. (10), $T = \sqrt{E^*/a}$ represents the nuclear temperature depending on the excitation energy E^* and the level density parameter a , $d = 0.3$ MeV is the rate of washing out the shell corrections with the temperature, and $T_0 = 1.16$ MeV is the value at which the damping factor $h(T)$ is reduced by 1/2. Analogously, in Eq. (11), $\Delta\ell = 3\hbar$ is the rate of washing out the shell corrections with the angular momentum, and $\ell_{1/2} = 20\hbar$ is the value at which the damping factor $q(\ell)$ is reduced by 1/2.

By regarding the determination of intrinsic level density ρ_{int} which takes into account the density of the intrinsic excitations, the nucleus is considered as a system made up to non-interacting Fermi gases (proton gas and neutron gas) at the same thermodynamic temperature T . It is supposed that each of the two gases is in thermodynamic equilibrium and that the excitation energy E^* is distributed in a statistical way between two gases. In this context for the intrinsic level density parameter

a we use the general expression [41] especially tailored to account for the shell effects in the level density

$$a(E^*) = \tilde{a} \left\{ 1 + \delta W \left[\frac{1 - \exp(-\gamma E^*)}{E^*} \right] \right\} \quad (12)$$

where $\tilde{a} = 0.094 \times A$ is the asymptotic value that takes into account the dependence on the mass number A , and $\gamma = 0.0064 \text{ MeV}^{-1}$ is the parameter which accounts for the rate at which shell effects wash out with excitation energy for neutron or other light particle emission. The general expression (12) works well also for deformed prolate or oblate nuclei. Physically, the disappearance of the shell effects with E^* excitation energy may be seen as a rearrangement of the shell-model orbitals in such a way that the shell gap between orbitals close to the Fermi energy vanishes. The value of the γ parameter was obtained [41] by fitting the observed density of neutron resonances.

In order to determine the a_{fis} level density parameter in the fission channel we use the relation $a_{fis}(E^*) = a_n(E^*) \times r(E^*)$ found in [42] where $r(E^*)$ is given by the relation

$$r(E^*) = \frac{\left[\exp(-\gamma_{fis} E^*) - \left(1 + \frac{E^*}{\delta W} \right) \right]}{\left[\exp(-\gamma E^*) - \left(1 + \frac{E^*}{\delta W} \right) \right]} \quad (13)$$

with $\gamma_{fis} = 0.024 \text{ MeV}^{-1}$. In Fig. 5 are reported, as an example, the values of the a_{fis}/a_n ratio versus E^* for two investigated reactions: (a) for the $^{48}\text{Ca} + ^{154}\text{Sm}$ reaction leading to the heavy ^{202}Pb CN* (red full line); (b) for the $^{26}\text{Mg} + ^{248}\text{Cm}$ reaction leading to the superheavy ^{274}Hs CN* (blue dashed line). At any excitation energy E^* the a_{fis}/a_n ratio is always greater than 1 and asymptotically tends to unity with increasing the excitation energy E^* at very high values.

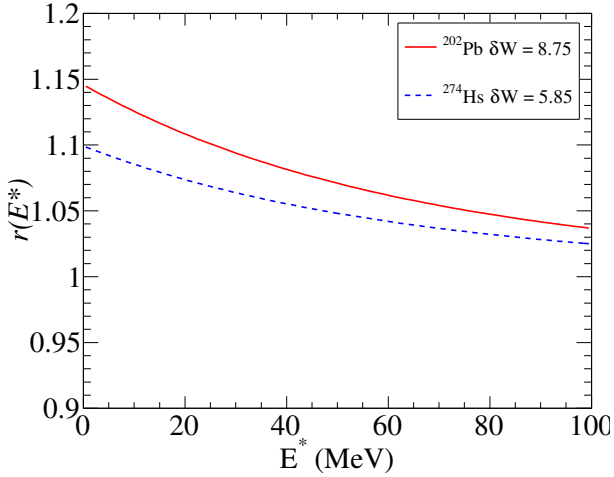


Figure 5: (Color on-line) The a_{fis}/a_n ratio vs E_{CN}^* for the two investigated reactions. Full line for the $^{48}\text{Ca} + ^{154}\text{Sm}$ reaction leading to the heavy ^{202}Pb CN and dashed line for the $^{26}\text{Mg} + ^{248}\text{Cm}$ reaction leading to the superheavy ^{274}Hs CN.

We stress that relation (13) allows one to describe in a consistent approach including collective effects the relevant functional form of the $a_{fis}(E^*)/a_n(E^*)$ ratio given by a general expression $r(E^*)$, rather than adjust by a phenomenological way

the value of the cited a_{fis}/a_n ratio for each excited nucleus. This procedure allows the shell corrections to become sensitive to the excitation energy, as shown in Fig. 6.

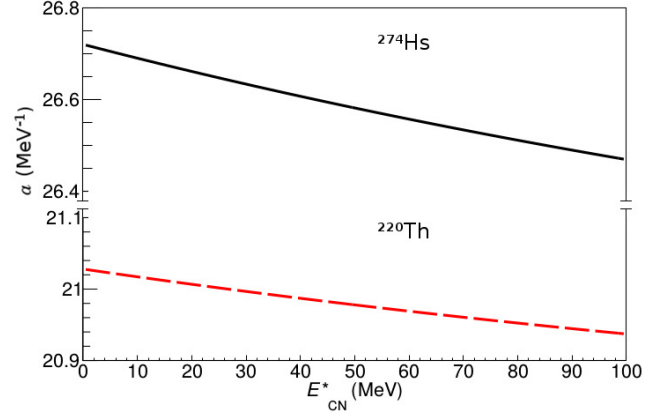


Figure 6: Level density parameter a vs E_{CN}^* for the ^{274}Hs CN obtained by the $^{26}\text{Mg} + ^{248}\text{Cm}$ reaction (full line) and the ^{220}Th CN obtained by the $^{16}\text{O} + ^{204}\text{Pb}$ reaction (dashed line).

To calculate the intrinsic level density $\rho_{int}(E^*, \ell)$ we use the general expression

$$\rho_{int}(E, J) = \frac{1}{16 \sqrt{6\pi}} \left[\frac{\hbar^2}{\mathcal{J}_{\parallel}} \right]^{1/2} a^{-1/4} \times \sum_{k=-J}^J [E - E_{rot}(k)]^{-5/4} e^{2\{a[E - E_{rot}(k)]\}^{1/2}} \quad (14)$$

where is

$$E_{rot}(k) = \frac{\hbar^2}{2\mathcal{J}_{\perp}} J(J+1) + \frac{\hbar^2 K^2}{2} \left[\frac{1}{\mathcal{J}_{\parallel}} - \frac{1}{\mathcal{J}_{\perp}} \right] \quad (15)$$

and where \mathcal{J}_{\perp} and \mathcal{J}_{\parallel} are moments of inertia perpendicular and parallel to the symmetry axis and K is the projection of the total spin J on the quantization axis. Application of the general expression [41] depends on the particular case. Specific cases take into account: the nucleus at the saddle point, the case of yrast state, and prolate or oblate or triaxial shape. This expression of ρ_{int} works well for both deformed and spherical nuclei as for example nuclei very close to the shell closure. The collective level density ρ_{coll} calculated in the adiabatic approach, valid at low excitation energies, takes into account in addition to the intrinsic excitations also the rotational and vibrational excitation states by the collective enhancement factor $K_{coll}(E^*)$:

$$\rho_{coll}^{adiab}(E^*, J) = \rho_{int}(E^*, J) \times K_{coll}^{adiab}(E^*)$$

where $K_{coll}^{adiab}(E^*)$ is given by the simple multiplication of the two $K_{rot}^{adiab}(E^*)$ and $K_{vibr}^{adiab}(E^*)$ enhancement factors; therefore, $\rho_{coll}^{adiab}(E^*, J)$ is determined (for more details see Appendix B) as

$$\rho_{coll}^{adiab}(E^*, J) = \rho_{int}(E^*, J) \times K_{rot}^{adiab}(E^*) \times K_{vibr}^{adiab}(E^*). \quad (16)$$

In Appendix B we give many other details regarding the intrinsic ρ_{int} and collective ρ_{coll} level density determinations, the fission Γ_{fis} and particle-x Γ_x decay widths, and we show the sensitivity of the model on final reaction products by using mass asymmetric and almost symmetric reactants in the entrance channel.

Moreover, if the capture of projectile by target takes place and complete fusion stage is reached, for the rotating mononucleus the fission barrier disappears at $\ell > \ell_{cr}$ (where ℓ_{cr} is a critical value characteristic for each nucleus) due to the damping of shell correction with angular momentum ℓ by the $q(\ell)$ function. To demonstrate the result of this effect, as an example, we present in Fig. 7(a) the W_{sur} survival probability vs ℓ regarding the deexcitation at first step of the ^{202}Pb CN formed in the $^{48}\text{Ca}+^{154}\text{Sm}$ reaction, at two different values of E_{CN}^* excitation energy of 46.5 and 65.6 MeV. This figure shows the sensitivity and importance of the ℓ angular momentum range on the W_{sur} surviving probability at the first step of deexcitation of the ^{202}Pb CN, and how its influence changes with increasing excitation energy. Therefore, the approximation often used in calculations of the fission barrier B_{fis} and W_{sur} surviving probability to fission for $\ell=0$ only leads to an insufficient ERs determination. Moreover, we present in Fig. 7 (b) W_{sur} vs E_{CN}^* for the same $^{48}\text{Ca}+^{154}\text{Sm}$ reaction leading to the ^{202}Pb CN. Even in this case, it is easy to observe the sensitivity of the W_{sur} function with the E_{CN}^* excitation energy: at high excitation energies ($E_{CN}^* > 70$ MeV) the W_{sur} value changes more than one order of magnitude with the change of the E_{CN}^* value of about 14 MeV and more than two orders of magnitude with the change of E_{CN}^* of about 23 MeV.

In addition, the panels (a) and (b) of Fig. 8 show the W_{sur} survival probability excitation functions for the ^{220}Th CN formed by the $^{16}\text{O}+^{204}\text{Pb}$ very asymmetric reaction and $^{124}\text{Sn}+^{96}\text{Zr}$ almost symmetric reaction, respectively.

By comparing the W_{sur} values obtained for two very different entrance channels leading to the formation of the ^{220}Th CN at excitation energies $E_{CN}^*=30, 40$ and 50 MeV, it is possible to observe the different effects of the angular momentum distribution on the surviving probability excitation functions. The W_{sur} values for the CN formed in the almost symmetric $^{124}\text{Sn}+^{96}\text{Zr}$ reaction are greater than the W_{sur} values corresponding to the one in the very asymmetric $^{16}\text{O}+^{204}\text{Pb}$ reaction by factors of 3.5, 4.2, and 4.5 times at the $E_{CN}^*=30, 40$ and 50 MeV, respectively. Certainly the increase of the beam energy $E_{c.m.}^*$ leads to an increase of the excitation energy E_{CN}^* of CN and to an extension of the angular momentum distribution of the CN formed in these reactions. But the behavior of the extension of the angular momentum distribution is different for the two reactions. The ℓ angular momentum range is larger for the ^{220}Th CN obtained in the very asymmetric $^{16}\text{O}+^{204}\text{Pb}$ reaction than for the CN obtained in the almost symmetric $^{124}\text{Sn}+^{96}\text{Zr}$ reaction at the same considered E_{CN}^* excitation energy. This difference in the angular momentum ℓ interval increases with the increase of E_{CN}^* since the size of the potential well in the nucleus-nucleus interaction for the almost symmetric $^{124}\text{Sn}+^{96}\text{Zr}$ reaction is smaller than the one for the very asymmetric reaction like $^{16}\text{O}+^{204}\text{Pb}$. Therefore, the number of the angular momentum ℓ contributing

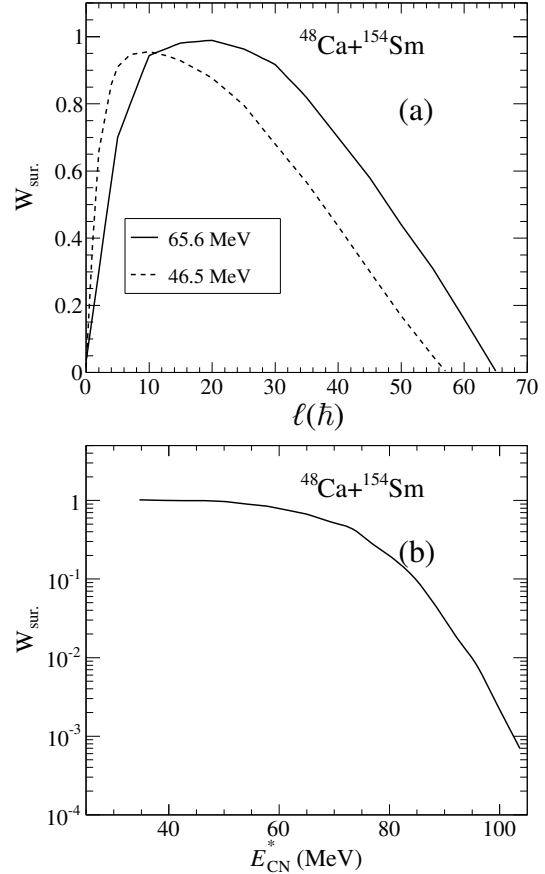


Figure 7: (a) The W_{sur} survival probability against fission of the deexcitation cascade of ^{202}Pb CN as a function of the ℓ angular momentum for the $^{48}\text{Ca}+^{154}\text{Sm}$ reaction at $E_{CN}^*=46.5$ (dashed line) and 65.6 MeV (full line) excitation energy of CN; (b) the W_{sur} survival probability against fission along the deexcitation cascade of ^{202}Pb CN as a function of the E_{CN}^* excitation energy for the same reaction.

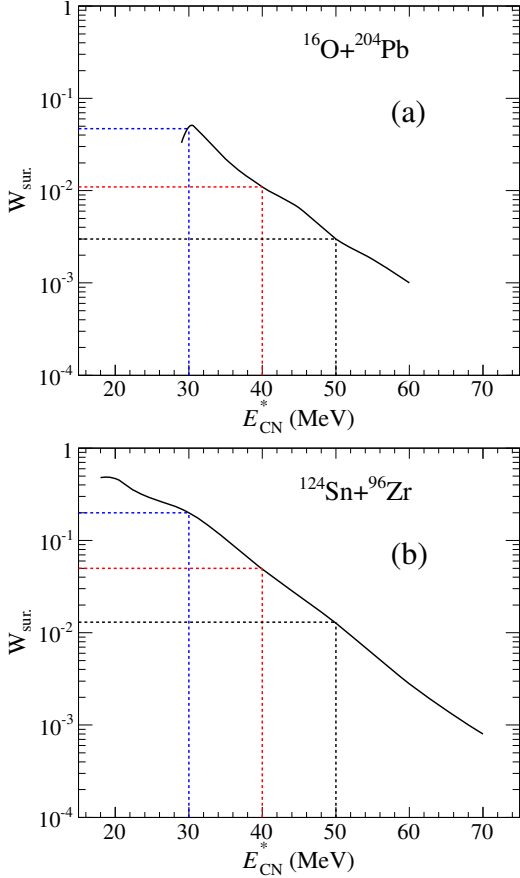


Figure 8: (Color on-line) (a) As Fig. 7 (b) but for the $^{16}\text{O}+^{204}\text{Pb}$ reaction leading to the ^{220}Th CN; (b) As Fig. 7 (b) but for the $^{124}\text{Sn}+^{96}\text{Zr}$ reaction leading to the same ^{220}Th CN.

to fusion in the $^{124}\text{Sn}+^{96}\text{Zr}$ reaction is smaller. Moreover, the fusion probability P_{CN} strongly decreases by increasing the angular momentum due to the increase of the B_{fus}^* intrinsic fusion barrier and due to a decrease of the B_{qf} quasifission barrier for the symmetric reaction (see for example ref. [43]). The quasifission barrier is the depth of the potential well in the nucleus-nucleus interaction (see Fig. A.10).

Obviously, the fusion cross section at a considered E_{CN}^* value of CN for the $^{124}\text{Sn}+^{96}\text{Zr}$ symmetric reaction is smaller than the one of the $^{16}\text{O}+^{204}\text{Pb}$ very asymmetric reaction, but with a smaller ℓ interval of the formed CN by the symmetric reaction has a greater W_{sur} survival probability to fission in comparison with the very asymmetric reaction.

Moreover, as discussed in our paper [33], it is difficult in experiment to estimate the σ_{ERtot} cross section when the emission of charged particles present also, because not all of residue nuclei can be identified. Therefore, apart from the uncertainties which are inherent to the theoretical predictions, there are ambiguities in the estimation of the fusion cross sections by the analysis of experimental data.

4. Conclusion

The reasons leading to uncertainties of the experimental and theoretical values of the fusion probability P_{CN} in heavy ion collision at lower energies are discussed. It should be stressed that there are two important reasons causing the uncertainties of the experimental values P_{CN} . The first reason is related to the ambiguity in identification of the reaction products formed by the true capture and fusion events. In the analysis of experimental data with full momentum transfer, events with masses around the values of light initial nucleus and conjugate nucleus are not usually taken into consideration. Those events are considered as originated by the deep-inelastic collisions and this procedure of the analysis leads to a decrease the experimental value of the capture cross section $\sigma_{cap}^{(exp)}$ and, consequently, to increase fusion probability P_{CN} since it inverse proportional to $\sigma_{cap}^{(exp)}$. The authors of ref. [15] considered the reaction products with mass numbers $A < 60$ as the ones of the deep-inelastic collisions and the capture events (characterized by the large energy dissipation and with a full momentum transfer) are missed. Therefore, the restriction of the mass range $60 \leq A \leq 130$ for the capture products is not completely correct because this assumption in the procedure of analysis of selection of experimental capture events leads to decrease the estimated true experimental capture cross sections. Therefore, the P_{CN} fusion probability determined by the analysis of experimental events as the ratio between the fusion and capture cross sections is bigger than the true experimental value. As a result the experimental fusion probability P_{CN} reported in Fig. 4 of ref. [21] unreasonably appear to be much higher with respect to the various theoretical determinations obtained by different theoretical models.

The second reason is the ambiguity in the separation of the fusion-fission events in the analysis of fission-like products containing quasifission or/and fast fission products. Therefore, the number of events seem to be larger than true fusion events due to consideration of the part of quasifission and fast fission events as fission events of compound nucleus which has not formed in the reaction. Certainly the extracted fusion probability P_{CN} will be larger than its correct value.

In fact, in reactions leading to superheavy compound nuclei, the yields of the quasifission and fast fission products are much more than the ones due to the fusion-fission products and, besides, the mass and the angular distributions of the reaction fragments can be strongly overlapped.

The authors of ref.[15] overestimated the fusion cross section by including quasifission events producing fragments with mass numbers in the range $60 \leq A \leq 130$. So the second reason of ambiguity in the identification of the reaction products also leads to an increase of the fusion probability P_{CN} in Fig. 4 of ref. [21]. The conclusion is that the good agreement between the experimental data and their theoretical description by the calculations of ref. [32] does not mean the success in study of the fusion-fission mechanism in the $^{48}\text{Ca}+^{154}\text{Sm}$ reaction. This question is still open and it must be studied by both the experimental and theoretical methods.

In order to check the reliability of an experimental result, it

would be good to be able to directly compare the deviations of the final results when they are made vary in a controlled manner the assumption made at the beginning of the analysis procedure. This methodology is widely used in other field of research, it is not however well practised in the complex study of reaction dynamics between heavy ions. Analogously, we demonstrate by figs. 7 and 8 the strong sensitivity of the W_{sur} surviving probability excitation function with the E_{CN}^* excitation energy and with the angular momentum ℓ values. In addition, due to difference in the spin distribution probability of the heated and rotating nucleus the survival probability W_{sur} is strongly sensitive to the kind of reactions in the entrance channel even if these reactions lead to the same CN formation with the same E_{CN}^* excitation energy.

We have explained the complexity of the fusion-fission and evaporation residue formation starting from the DNS formation in the entrance channel. It is important to take into account the role of the intrinsic fusion barrier B_{fus}^* and quasifission barrier B_{qf} in the complete fusion/ quasifission competition that are sensitive to the DNS lifetime and angular momentum range. Moreover, the fast fission products caused by the decay of the complete fusion deformed mononucleus with high angular momentum values ℓ (because $B_{\text{fis}} = 0$ for $\ell > \ell_{\text{cr}}$) before reaching the statistically equilibrated shape of CN, intensively populate the symmetric mass distribution at higher E_{CN}^* excitation energies. Thus, these experimental determinations and extracted P_{CN} fusion probabilities appear strongly overestimated (see the experimental results in Fig. 1 taken from refs.[22, 23]).

On the other hand, it is not realistic to admit as a reliable result that the ratio between the P_{CN} values deduced from experimental observations of the very asymmetric reaction $^{26}\text{Mg}+^{248}\text{Cm}$ leading to CN with $Z_{\text{CN}} = 108$ ($P_{\text{CN}}(Z = 108)$) and the one deduced from the less asymmetrical reaction $^{86}\text{Kr}+^{208}\text{Pb}$ leading to CN with $Z_{\text{CN}} = 118$ ($P_{\text{CN}}(Z = 118)$), respectively, is $P_{\text{CN}}(Z = 108)/P_{\text{CN}}(Z = 118) = 0.31 \times 10^{-1}$, while the analogous ratio $P_{\text{CN}}(Z = 108)/P_{\text{CN}}(Z = 118)$ between P_{CN} theoretical values is 0.23×10^{-4} indicating a ratio between experimental and theoretical values that is at least 3 orders of magnitude higher. Similarly, the variation of P_{CN} deduced from the experiments for the $^{48}\text{Ca}+^{208}\text{Pb}$ ($\eta = 0.63$ and $Z_{\text{CN}} = 102$) and $^{58}\text{Fe}+^{248}\text{Cm}$ ($\eta = 0.63$ and $Z_{\text{CN}} = 122$) reactions, having the same asymmetry parameters η , is approximately one order of magnitude, while the theoretical results indicate a change of about four orders of magnitude. If these theoretical predictions were completely unreliable, then it remains incomprehensible why with an experimental change of P_{CN} of about one order of magnitude, the cross sections of evaporation residues pass from values of μb to that of pb and also much less (about 10 fb) such as it is impossible to detect events of evaporation residues.

The characteristics of our model and procedure used for calculation are based on the possibility to analyze the different evolution of various nuclear reactions in the entrance channel with the use of one radius parameter r_0 to study different reactions. The sensitivity of fusion probability is discussed in Appendix A of this work. Moreover, in the model all properties of reaction which are responsible for the evolution of reactants with formation of intermediate states and final products (potentials,

barriers, excitation function, reaction mechanisms, competition of processes, cross sections, etc.) are considered as dependent on the energy and angular momentum. We have shown that the consistent description of the fission cross section reached by consideration of the fade-out of the shell correction to the fission barrier with increasing temperature and angular momentum. This result is of crucial importance for the synthesis of the superheavy elements, since it extends the stabilizing effects of the shell structure to higher temperatures, but this stabilizing effect, however, will be partially removed by the decrease of the shell correction with the increasing angular momentum. Moreover, we note that the investigation of the temperature dependence of the shell correction might be extended to the analysis of the photofission reactions, in which the angular momentum effects are practically absent. We also have given in the paper a general expression allowing for the determination of the $a_{\text{fis}}(E^*)/a_{\text{n}}(E^*)$ ratio, valid both for spherical and deformed nuclei, and we discussed about the role and modalities of the enhancement factors in the level density at lower and higher excitation energies. Therefore, the sensitivity and reliability of our modular system of nuclear reaction codes, starting from the contact of reactants in the entrance channel to the formation of final products, have been shown in detail in order to take into account various reaction mechanisms present at different steps of reaction characterized by different entrance channels. This means that all properties of reacting nuclei are considered, the orientation angle between the symmetry axes of deformed reactants are taken into account in order to estimate the real Coulomb barrier between reacting nuclei as a function of the beam energy at the stage of contact. Moreover, the role of the driving potential as a function of energy and angular momentum is considered, the dependence of the intrinsic fusion barrier $B_{\text{fus}}^*(E^*, \ell)$ and the quasifission $B_{\text{qf}}(E^*, \ell)$ barrier are detailed in order to calculate the fusion probability P_{CN} , the fusion and quasifission cross sections; moreover, the complete deexcitation cascade of CN is analyzed in order to calculate at each step the fission and ER cross sections where the fission barrier and the shell effects are determined by using the damping functions $h(T)$ and $q(\ell)$ in the competition between light-particle emission and fission processes when the light charged particles are also considered. Therefore, such our modular system of codes for the study nuclear reactions also represents a powerful predictive theoretical way for new investigations also giving the limits of the reliable expectation.

Instead, in our conclusion, we affirm that the desire to find a phenomenological model or a simple theoretical model in order to have a detailed knowledge about the reaction dynamics in heavy ion collisions and the clear characteristics of the reaction products is a vain hope. It was believed that it would be enough to make the so-called ‘‘reasonable’’ assumptions in treatment of data or in application of models with the aim of simplifying the problem, but in reality the obtained results were strongly affected by large uncertainties as we have explained in ref. [33]. Therefore, a simplified and unsuitable model leads to an unhelpful information as it does not provide a realistic understanding of the phenomenon which one wants to study.

Appendix A. Procedures for determination of P_{CN}

The ratio of the sum of the evaporation residue and fusion-fission cross sections to the capture cross section is used to extract the fusion probability from the experimental data of the reaction products (see expression (1) in Introduction). It is clear that the experimental results are a sum of contributions from the reactions taking place in collisions with different values of the orbital angular momentum. Therefore, the fusion probability depends on the orbital angular momentum since the intrinsic fusion barrier B_{fus}^* and quasifission B_{qf}^* barriers are its function. The partial capture cross section is calculated by the estimation of the range of the orbital angular momentum leading to the full momentum transfer in the entrance channel of collision. This procedure is realized by solution of the equations of motion for the relative distance between the centres-of-mass of colliding nuclei and orbital angular momentum with the radial and tangential friction coefficients.

$$\mu(R) \frac{d\dot{R}}{dt} + \gamma_R(R) \dot{R}(t) = F(R), \quad (A.1)$$

$$F(R) = -\frac{(\partial V(R) + \delta V(R))}{\partial R} - \dot{R}^2 \frac{\partial \mu(R)}{\partial R}, \quad (A.2)$$

$$\frac{dL}{dt} = \gamma_\theta(R) R(t) (\dot{\theta} R(t) - \dot{\theta}_1 R_{1eff} - \dot{\theta}_2 R_{2eff}), \quad (A.3)$$

$$L_0 = J_R \dot{\theta} + J_1 \dot{\theta}_1 + J_2 \dot{\theta}_2, \quad (A.4)$$

$$E_{rot} = \frac{J_R \dot{\theta}^2}{2} + \frac{J_1 \dot{\theta}_1^2}{2} + \frac{J_2 \dot{\theta}_2^2}{2}, \quad (A.5)$$

where $R \equiv R(t)$ is the relative motion coordinate; $\dot{R}(t)$ is the corresponding velocity; L_0 and E_{rot} are defined by initial conditions; J_R and $\dot{\theta}$, J_1 and $\dot{\theta}_1$, J_2 and $\dot{\theta}_2$ are moment of inertia and angular velocities of the DNS and its fragments, respectively (J_R , J_1 and J_2 are defined in Ref. [44]); γ_R and γ_θ are the friction coefficients for the relative motion along R and the tangential motion when two nuclei roll on each other's surfaces, respectively; $V(R)$ is the nucleus-nucleus potential which includes Coulomb, nuclear and rotational potentials (see Eq.(A.1) Ref. [18, 44]); $\mu(R, t)$ is the reduced mass of the system:

$$\mu(R, t) = \tilde{\mu}(R, t) + \delta\mu(R, t), \quad (A.6)$$

where

$$\tilde{\mu}(R, t) = m_0 A_T(R, t) \cdot A_P(R, t) / (A_T(R, t) + A_P(R, t)),$$

at $t = 0$ $A_T(R)$ and $A_P(R)$ are equal to mass numbers of the target- and projectile-nucleus, respectively; m_0 is the nucleon mass. The time dependencies of $A_P(t) = Z_P(t) + N_P(t)$ and $A_T(t) = Z_T(t) + N_T(t)$ are found by solution of master equation for the evolution of occupation numbers of single-particle states in nuclei as in [18]; $\delta V(R)$ and $\delta\mu(R, t)$ are changes of the interaction potential $V(R)$ and reduced mass μ , respectively, during interaction due to nucleon exchange and overlap of nucleon densities of interacting nuclei (see Ref. [44]);

$$R_{1(2)eff} = \frac{R_{01(02)}}{R_{01} + R_{02}} R,$$

where $R_{01(02)}$ is the nucleus equilibrium radius: $R_{0i} = r_0 A_i^{1/3}$, $r_0 = 1.18$ fm.

The use of the friction coefficients related with the excitation of intrinsic degrees of freedom allows us to separate trajectories of the deep-inelastic collisions and full momentum transfer reactions (see Fig. A.9).

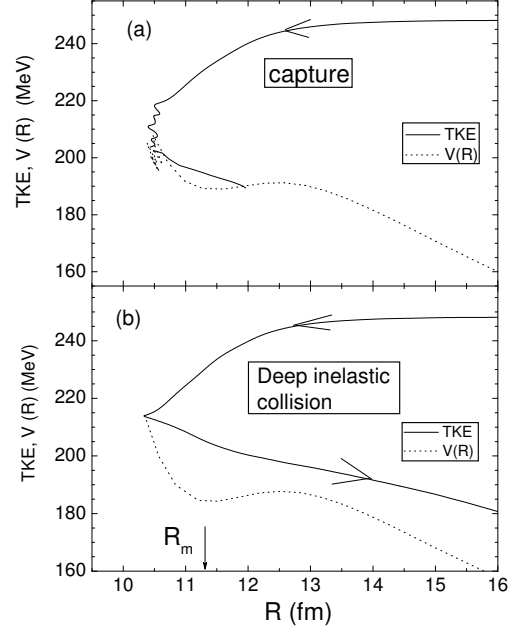


Figure A.9: The difference between capture (a) and deep inelastic collision (b) caused by the dependence of the dissipation of the total kinetic energy of the relative motion and the nucleus-nucleus potential on the radial distance and orbital angular momentum L for the $^{48}\text{Ca}+^{208}\text{Pb}$ reaction at heavy ion collisions with $L_0 = 40\hbar$ (a) and $20\hbar$ (b) at $E_{c.m.}=248$ MeV.

The partial capture cross section is determined by the capture probability $\mathcal{P}_{cap}^{(\ell)}(E)$ which means that the colliding nuclei are trapped into the well of the nucleus-nucleus potential after dissipation of a part of the initial kinetic energy and orbital angular momentum:

$$\sigma_{cap}^{(\ell)}(E, \alpha_1, \alpha_2) = \pi \lambda^2 \mathcal{P}_{cap}^{(\ell)}(E, \alpha_1, \alpha_2) \quad (A.7)$$

Here λ is the de Broglie wavelength of the entrance channel. The capture probability $\mathcal{P}_{cap}^{(\ell)}(E, \alpha_1, \alpha_2)$ is equal to 1 or 0 for the given beam energy and orbital angular momentum. Our calculations showed that in dependence on the beam energy, $E = E_{c.m.}$, there is a window for capture as a function of orbital angular momentum (α_1 and α_2 are omitted here for the simplicity of the formula):

$$\mathcal{P}_{cap}^{(\ell)}(E) = \begin{cases} 1, & \text{if } \ell_{min} < \ell < \ell_d \text{ and } E > V_{Coul} \\ 0, & \text{if } \ell > \ell_d \text{ or } \ell < \ell_{min} \text{ and } E > V_{Coul} \\ 0, & \text{for all } \ell \text{ if } E \leq V_{Coul}, \end{cases}$$

where $\ell_{min} \neq 0$ can be observed when the beam energy is large than the Coulomb barrier (V_{Coul}).

While exists the DNS formed at capture, we have an ensemble $\{Z\}$ of the DNS configurations which contributes to the competition between complete fusion and quasifission with probabilities $\{Y_Z\}$. The dependence of barrier B_{fus}^* and excitation

energy of DNS E_Z^* for given charge Z and mass A on angular momentum and orientation angles α_i ($i = 1, 2$) of the symmetry axis of interacting nuclei is connected with the method of calculation of the interacting potential between nuclei of DNS which is sensitive to those variables. Consequently, the fusion factor P_{CN} for the given reaction depends on the same variables through the charge distribution $Y_Z(E_Z^*)$ and fusion factor $P_{CN}^{(Z)}$ from charge asymmetry configuration Z :

$$P_{CN}(E_Z^*, \ell; \alpha_1, \alpha_2) = \sum_{Z_{sym}}^{Z_{max}} Y_Z(E_Z^*, \ell) P_{CN}^{(Z)}(E_Z^*, \ell; \alpha_1, \alpha_2), \quad (\text{A.8})$$

where $P_{CN}^{(Z)}(E_Z^*, \ell; \alpha_1, \alpha_2)$ is the fusion probability for DNS having excitation energy E_Z^* at charge asymmetry Z and orientation angles of symmetry axis of its fragments are equal to α_1 and α_2 . The evolution of Y_Z is calculated by solving the transport master equation:

$$\begin{aligned} \frac{\partial}{\partial t} Y_Z(E_Z^*(\ell), t) &= \Delta_{Z+1}^{(-)} Y_{Z+1}(E_Z^*(\ell), t) + \\ &\Delta_{Z-1}^{(+)} Y_{Z-1}(E_Z^*(\ell), t) - (\Delta_Z^{(-)} + \Delta_Z^{(+)} + \Lambda_Z^{qf}) Y_Z(E_Z^*(\ell), t), \end{aligned} \quad (\text{A.9})$$

for $Z = 2, 3, \dots, Z_{tot} - 2$.

Here, the transition coefficients of multinucleon transfer are calculated as in Ref. [45]

$$\begin{aligned} \Delta_Z^{(\pm)} &= \frac{1}{\Delta t} \sum_{PT} |g_{PT}^{(Z)}|^2 n_{T,P}^{(Z)}(E_Z^*(\ell), t) (1 - n_{P,T}^{(Z)}(E_Z^*(\ell), t)) \\ &\frac{\sin^2(\Delta t(\varepsilon_{Pz} - \varepsilon_{Tz})/2\hbar)}{(\varepsilon_{Pz} - \varepsilon_{Tz})^2/4}, \end{aligned} \quad (\text{A.10})$$

where ε_{iz} and $n_i^{(Z)}(E_Z^*(\ell), t)$ are the single-particle energies and occupation numbers of nucleons in the DNS fragments; the matrix elements g_{PT} describe one-nucleon exchange between the nuclei of DNS, and their values are calculated microscopically using the expression obtained in Ref. [46]. The decay probability of DNS Λ_Z^{qf} from the charge asymmetry configuration Z is calculated by the formula used in Ref. [47]:

$$\begin{aligned} \Lambda_Z^{qf} &= K_{rot}(E_Z^*) \omega_m \left(\sqrt{\gamma^2/(2\mu_{qf})^2 + \omega_{qf}^2} - \gamma/(2\mu_{qf}) \right) \\ &\times \exp(-B_{qf}/T_Z(\ell)) / (2\pi\omega_{qf}), \end{aligned} \quad (\text{A.11})$$

where, $T_Z(\ell)$ is the effective temperature of DNS and it is estimated by formula:

$$T_Z = \sqrt{\frac{E_{DNS}^{(Z)}}{a_{DNS}}}, \quad (\text{A.12})$$

which is determined by the DNS excitation energy $E_{DNS}^{(Z)} = E_{c.m.} - V_{min}(R) + Q_{gg}^{(Z)}$ and by the corresponding level density parameter: $a_{DNS} = A/12 \text{ MeV}^{-1}$. The dependence the DNS excitation energy on the charge asymmetry is related with the change of its intrinsic energy by the change of mass and charge numbers of its constituents from the ones of projectile and target nuclei:

$$\begin{aligned} Q_{gg}^{(Z)} &= B_1(Z_P, A_P) + B_2(Z_T, A_T) - \\ &B_1(Z, A) - B_2(Z_{CN} - Z, A_{CN} - A), \end{aligned} \quad (\text{A.13})$$

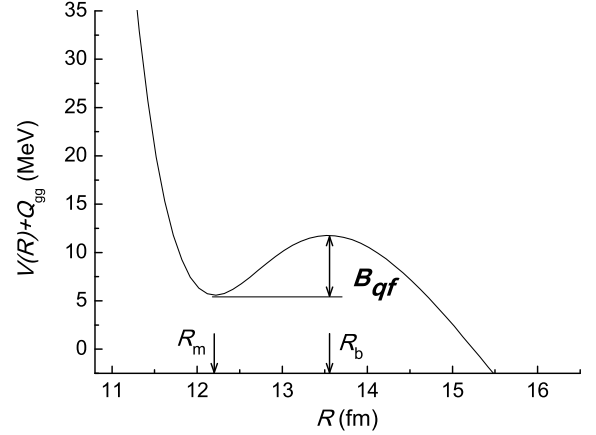


Figure A.10: The nucleus-nucleus interaction potential $V(R)$ for the $^{19}\text{F}+^{208}\text{Pb}$ system: the quasifission barrier B_{qf} as the a depth of the potential well.

Here the frequency ω_m and ω_{qf} are found by the harmonic oscillator approximation to the nucleus-nucleus potential $V(R)$ shape for the given DNS configuration ($Z, Z_{tot}-Z$) on the bottom of its pocket placed at R_m and on the top (quasifission barrier) placed at R_{qf} (see Fig. A.10), respectively:

$$\omega_m^2 = \mu_{qf}^{-1} \left. \frac{\partial^2 V(R)}{\partial R^2} \right|_{R=R_m}, \quad (\text{A.14})$$

$$\omega_{qf}^2 = \mu_{qf}^{-1} \left. \frac{\partial^2 V(R)}{\partial R^2} \right|_{R=R_{qf}}. \quad (\text{A.15})$$

The collective enhancement factor of the rotational motion K_{rot} to the level density should be included because the dinuclear system is a good rotator. It is calculated by the well known expression [54]:

$$K_{rot}(E_Z^*) = \begin{cases} (\sigma_{\perp}^2 - 1)f(E_Z^*) + 1, & \text{if } \sigma_{\perp} > 1 \\ 1, & \text{if } \sigma_{\perp} \leq 1, \end{cases}$$

where $\sigma_{\perp} = J_{DNS} T / \hbar^2$; $f(E) = (1 + \exp[(E - E_{cr})/d_{cr}])^{-1}$; $E_{cr} = 120\tilde{\beta}_2^2 A^{1/3} \text{ MeV}$; $d_{cr} = 1400\tilde{\beta}_2^2 A^{2/3}$. $\tilde{\beta}$ is the effective quadrupole deformation for the dinuclear system. We find it from the results of $\mathcal{J}_{\perp}^{DNS}$ calculated as in Ref. [47].

The fusion probability $P_{CN}^{(Z)}(E_Z^*(\ell); \{\alpha_i\})$ is calculated by the expression (A.16) presented in our work [8]:

$$P_{CN}^{(Z)}(E_Z^*(\ell)) = \frac{\rho_{fus}(E_Z^*(\ell))}{\rho_{fus}(E_Z^*(\ell)) + \rho_{qf}(E_Z^*(\ell)) + \rho_{sym}(E_Z^*(\ell))}. \quad (\text{A.16})$$

The level density of DNS was calculated by formula from Ref. [48]

$$\begin{aligned} \rho_i(E_Z^*) &= \left[\frac{g^2}{g_1 g_2} \right]^{1/2} \exp \left[2(a(E_Z^* - B_i)^{1/2}) \right] \\ &\cdot \frac{g}{6^{3/4} (2a(E_Z^* - B_i)^{5/4})}, \end{aligned} \quad (\text{A.17})$$

where $i = \text{fus, qf, sym}$; g_1 and g_2 are densities of single-particle states near the Fermi surface for the DNS nuclei; $2g = g_1 + g_2$,

and $a = \pi^2/6g$. We used the following set of parameters: $g = g_1 = g_2$ and $a = A/12 \text{ MeV}^{-1}$.

In the DNS model the hindrance to complete fusion is determined by the peculiarities of the driving potential which is calculated as a sum of the reaction energy balance Q_{gg} and interaction potential between the DNS nuclei:

$$U_{\text{dr}}(A, Z, \ell) = Q_{gg} + V(Z_1, A_1, Z_2, A_2, \ell, \{\alpha_i\}; R), \quad (\text{A.18})$$

where $Q_{gg} = B_1 + B_2 - B_{\text{CN}}$, B_1 , B_2 and B_{CN} are the binding energies of the interacting nuclei and CN, respectively, which are obtained from the nuclear mass tables in Refs. [37, 49].

The nucleus-nucleus potential V consists of the three parts:

$$\begin{aligned} V(Z_1, A_1, Z_2, A_2, \ell, \{\alpha_i\}; R) = & \\ & V_{\text{Coul}}(Z_1, A_1, Z_2, A_2, \{\alpha_i\}; R) \\ & + V_{\text{nucl}}(Z_1, A_1, Z_2, A_2, \{\alpha_i\}; R) \\ & + V_{\text{rot}}(Z_1, A_1, Z_2, A_2, \ell, \{\alpha_i\}; R), \end{aligned} \quad (\text{A.19})$$

where V_{Coul} , V_{nucl} , and V_{rot} are the Coulomb, nuclear, and rotational potentials, respectively. The Coulomb potential $V_{\text{Coul}}(R)$ is calculated by Wong's formula [50]:

$$\begin{aligned} V_{\text{C}}(R, \alpha_1, \alpha_2) = & \frac{Z_1 Z_2}{R} e^2 \\ & + \frac{Z_1 Z_2}{R^3} e^2 \left\{ \left(\frac{9}{20\pi} \right)^{1/2} \sum_{i=1}^2 R_{0i}^2 \beta_2^{(i)} P_2(\cos \alpha'_i) \right. \\ & \left. + \frac{3}{7\pi} \sum_{i=1}^2 R_{0i}^2 [\beta_2^{(i)} P_2(\cos \alpha'_i)]^2 \right\}, \end{aligned} \quad (\text{A.20})$$

where $\alpha'_1 = \alpha_1 + \Theta$, $\alpha'_2 = \pi - (\alpha_2 + \Theta)$, $\sin \Theta = |\mathbf{L}|/(\mu R \dot{R})$; Z_i , $\beta_2^{(i)}$, and α'_i are the atomic number (for each fragment), the quadrupole deformation parameter, and the angle (see Fig.A.11) between the line connecting the centers of masses of the nuclei and the symmetry axis of the fragment i ($i = 1, 2$), respectively. Here, $P_2(\cos \alpha'_i)$ is the second term of the second type of Legendre polynomial. The radius parameter r_0 used to find the nuclear radius $R_{0i} = r_0 A_i^{1/3}$ is changed in the range $r_0 = 1.16$ — 1.17 fm to reach an agreement with the experimental data of the capture cross section at lowest energies.

The nuclear part of the nucleus-nucleus potential is calculated using the folding procedure between the effective nucleon-nucleon forces $f_{\text{eff}}[\rho(x)]$ suggested by Migdal [51] and the nucleon density of the projectile and target nuclei, $\rho_1^{(0)}$ (A.24) and $\rho_2^{(0)}$ (A.23), respectively:

$$\begin{aligned} V_{\text{nucl}}(R, \alpha_1, \alpha_2) = & \int \rho_1^{(0)}(\mathbf{r} - \mathbf{R}; \alpha_1, \beta_2^{(1)}) f_{\text{eff}}[\rho] \\ & \times \rho_2^{(0)}(\mathbf{r}; \alpha_2, \beta_2^{(2)}) d^3 \mathbf{r}, \end{aligned} \quad (\text{A.21})$$

$$f_{\text{eff}}[\rho] = 300 \left(f_{\text{in}} + (f_{\text{ex}} - f_{\text{in}}) \frac{\rho(0) - \rho(r)}{\rho(0)} \right). \quad (\text{A.22})$$

Here $f_{\text{in}} = 0.09$, $f_{\text{ex}} = -2.59$ are the constants of the effective nucleon-nucleon interaction; $\rho = \rho_1^{(0)} + \rho_2^{(0)}$. The center of the laboratory coordinate system is placed on the target mass center and, therefore, $r_1 = R$ and $r_2 = 0$.

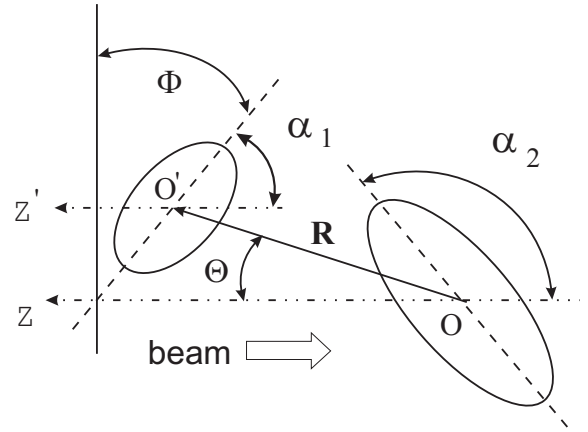


Figure A.11: The coordinate systems and angles which were used for the description of the initial orientations of projectile and target nuclei. The beam direction is opposite to OZ .

The angles between the symmetry axis of the projectile and target nucleus and the beam direction are α_1 and α_2 , respectively, (Fig.A.11). The spherical coordinate system O with the vector r , angles θ and ϕ is placed at the mass center of the target nucleus and the Oz axis is directed opposite to the beam. In this coordinate system, the direction of the vector \mathbf{R} connecting the mass centers of the interacting nuclei has angles Θ and Φ : $\mathbf{r}_1 = \mathbf{R}$ and $\mathbf{r}_2 = 0$. The coordinate system is chosen in such a way that the planes, in which the symmetry axes of nuclei are located, cross the Oz line and form the angle Φ . For head-on (or polar) collisions $\Theta = 0$ and $\Phi = \phi$.

In this context we present in Fig A.12 for the $^{48}\text{Ca} + ^{154}\text{Sm}$ reaction the dependence of the Coulomb barrier V_{C} on the initial orientation angle α_{T} of the symmetry axis of target nucleus with respect to the beam direction that it is necessary to consider in determination of nucleus-nucleus potential V (see formula (A.19)). In this present case, when the beam-target interaction occurs with an angle $\alpha_{\text{T}} = 0^\circ$ of the target (tip collision), the Coulomb barrier V_{C} is characterized by the minimum value of about 124 MeV; instead, V_{C} reaches the maximum value of about 148.2 MeV when the beam interacts with target with an angle $\alpha_{\text{T}} = 90^\circ$ (equatorial collision). In this last case the Coulomb barrier value is about 20% higher than the one in the $\alpha_{\text{T}} = 0^\circ$ target orientation. In our paper [9] we analyzed in detail the contributions of the capture and fusion cross sections versus the collision energy $E_{\text{c.m.}}$ for various target orientation angles α_{T} , and we presented the results of calculation in Fig.3 of the cited paper [9]. At lower $E_{\text{c.m.}}$ energies (at about $E_{\text{c.m.}} < 137$ MeV, only the small orientation angle of the target ($\alpha_{\text{T}} \leq 45^\circ$) can contribute to the capture cross section due to the low values of the Coulomb barrier for the mentioned α_{T} angle range. At $E_{\text{c.m.}} = 148$ MeV, all the α_{T} configurations can contribute to the capture cross section with approximately the same possibilities because the collision energy $E_{\text{c.m.}}$ is sufficient to overcome the maximum value of the Coulomb barrier, depending on the α_{T} angle orientation at initial contact of reactants; instead, at the above-mentioned low energy range $E_{\text{c.m.}} < 137$ MeV the fusion cross section can only be contributed by a small set of orien-

tation angles of the target with $\alpha_T \leq 45^\circ$ at initial beam-target interaction. At higher $E_{c.m.}$ energies (at about $E_{c.m.} > 155$ MeV) the contributions to the configurations with $\alpha_T > 45^\circ$ are larger than those with $\alpha_T \leq 30^\circ$ for both capture and fusion cross sections (see Ref. [9] for other important details).

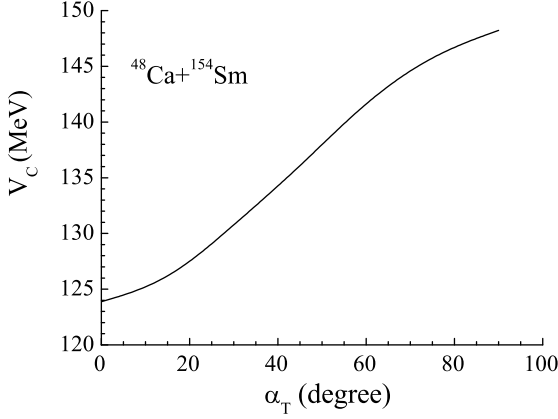


Figure A.12: Coulomb barrier V_C of the nucleus-nucleus interaction vs the orientation angle α_T of the target-nucleus for the $^{48}\text{Ca}+^{154}\text{Sm}$ reaction.

The shape of the dinuclear system nuclei changes with the evolution of the mass asymmetry degrees of freedom: $\beta_2 = \beta_2(Z, A)$ and $\beta_3 = \beta_3(Z, A)$. In order to calculate the potential energy surface as a function of the charge number, we use the values of $\beta_2^{(2^+)}$ from [52] and the values of $\beta_3^{(3^-)}$ from [53]. In the O system the symmetry axis of the target-nucleus is turned around the α_2 angle, so its nucleon distribution function is as follows:

$$\rho_2^{(0)}(r) = \rho_0 \left\{ 1 + \exp \left[\frac{r - \tilde{R}_2(\beta_2^{(2)}, \beta_3^{(2)}; \theta_2)}{a} \right] \right\}^{-1}, \quad (\text{A.23})$$

$$\tilde{R}_2(\beta_2^{(2)}, \beta_3^{(2)}; \theta_2) = R_0^{(2)} \left(1 + \beta_2^{(2)} Y_{20}(\theta_2) + \beta_3^{(2)} Y_{30}(\theta_2) \right),$$

where $\rho_0 = 0.17 \text{ fm}^{-3}$, $a_0 = 0.54 \text{ fm}$,

$$\cos \theta_2 = \cos \theta \cos(\pi - \alpha_2) + \sin \theta \sin(\pi - \alpha_2) \cos \phi.$$

The mass center of the projectile nucleus is shifted to the end of the vector R and its symmetry axis is turned by the angle $\pi - \alpha_1$. According to the transformation formulae of the parallel transfer of vectors the variables of the transferred system O' are as follows:

$$\begin{aligned} r'^2 &= r^2 + R^2 - 2rR \cos(\omega_{12}), \\ \cos(\omega_{12}) &= \cos \theta \cos \Theta + \sin \theta \sin \Theta \cos(\phi - \Phi), \\ \cos \theta'_1 &= \frac{(r \cos \theta - R \cos \Theta)}{r'}, \\ \cos \phi'_1 &= (1 + \tan^2 \phi'_1)^{-1/2}, \\ \tan \phi'_1 &= \frac{r \sin \phi \sin \theta - R \sin \Theta \sin \Phi}{r \cos \phi \sin \theta - R \sin \Theta \cos \Phi}. \end{aligned}$$

In the coordinate system O' , the deviation of the symmetry axis of projectile nuclei relative to the $O'z'$ axis is determined by the

angle

$$\cos \theta''_1 = \cos \theta'_1 \cos(\pi - \alpha_1) + \sin \theta'_1 \cos \phi'_1.$$

Now the nucleon distribution function of the projectile-nucleus looks like this

$$\rho_1^{(0)}(r') = \rho_0 \left\{ 1 + \exp \left[\frac{r' - \tilde{R}_1(\beta_2^{(1)}, \beta_3^{(1)}; \theta'_1)}{a} \right] \right\}^{-1}, \quad (\text{A.24})$$

$$\tilde{R}_1(\beta_2^{(1)}, \beta_3^{(1)}; \theta'_1) = R_0^{(1)} \left(1 + \beta_2^{(1)} Y_{20}(\theta'_1) + \beta_3^{(1)} Y_{30}(\theta'_1) \right).$$

The sensitivity of the driving potential U_{dr} and quasifission barrier B_{qf} to the change of the radius parameter is presented in Fig. A.13 and A.14, respectively.

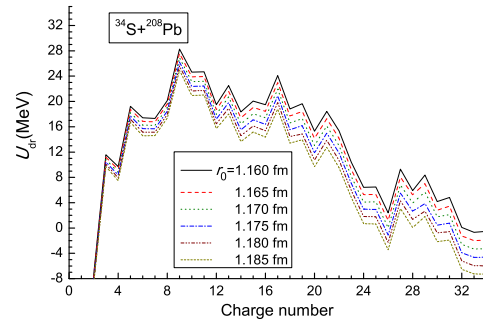


Figure A.13: (Color on-line) The dependence of the driving potential calculated for the $^{36}\text{S}+^{206}\text{Pb}$ reaction on the values of the radius parameter r_0 .

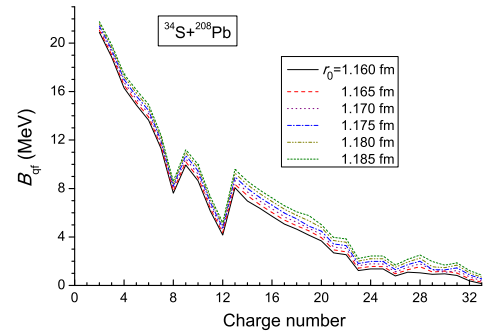


Figure A.14: (Color on-line) The dependence of the quasifission barrier calculated for the $^{36}\text{S}+^{206}\text{Pb}$ reaction on the values of the radius parameter r_0 .

The sensitivity of the capture σ_{cap} and fusion σ_{fus} cross sections to the change of the radius parameter is presented in Fig. A.15 and A.16, respectively, while the sensitivity of the P_{CN} fusion probability is about 2 times at low beam energies $E_{c.m.} = 136-140$ MeV. Instead, at higher beam energies $E_{c.m.} \geq 145$ MeV the P_{CN} values are approximately insensitive to the change of r_0 from 1.16 fm to 1.18 fm (see Fig. A.17).

As a result the position, slope and values of the capture and fusion excitation functions are changed significantly, while the P_{CN} fusion probability changes a little. Moreover, as one can see that the shift of the excitation function is about 3 MeV at lowest energies at the change of r_0 from 1.16 fm to 1.18 fm. This property of the excitation function is used in our calculation to reach an agreement of the capture cross section at the lowest energies with the experimental data. Usually we necessity of the shift of the position of the curve of excitation functions no more 3 MeV.

We should note that the partial fusion cross sections are used in calculation of the survival probability of the excited compound nucleus. It is important to take into account the dependence of the fission barrier on the angular momentum.

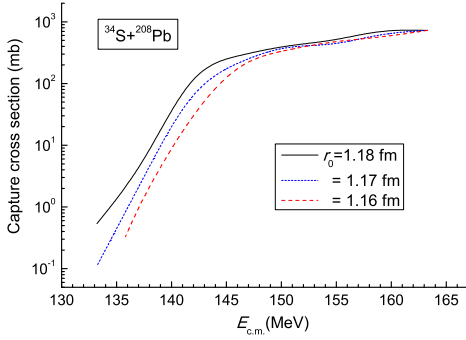


Figure A.15: (Color on-line) The capture cross section σ_{cap} calculated for the $^{34}\text{S}+^{208}\text{Pb}$ reaction on the values of the radius parameter r_0 .

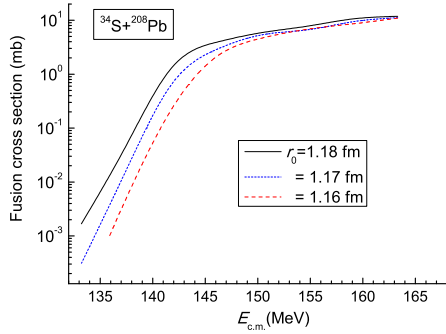


Figure A.16: (Color on-line) The dependence of the fusion cross section calculated for the $^{34}\text{S}+^{208}\text{Pb}$ reaction on the values of the radius parameter r_0 .

Appendix B. Procedures for determination of final products of CN

In our model and procedures, the calculation of the effective fission barrier B_{fis} is a function of the nuclear temperature

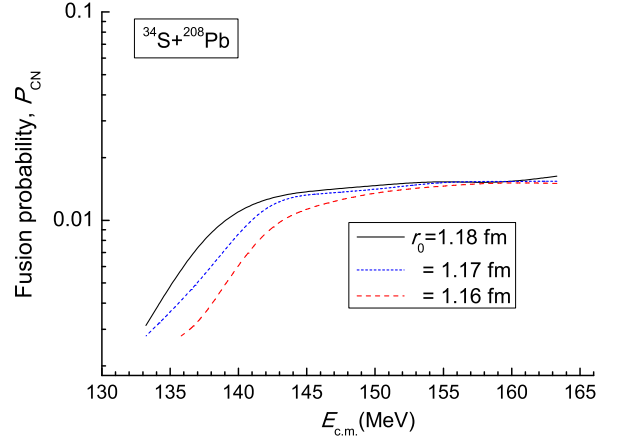


Figure A.17: The dependence of the fusion probability P_{CN} calculated for the $^{34}\text{S}+^{208}\text{Pb}$ reaction on the values of the radius parameter r_0 .

T and angular momentum ℓ as indicated in formula (9) of the paper. The damping function for the washing out of shell effect works in a very good way for general cases of heavy and superheavy compound nuclei reached by heavy-ion reactions by comparing our theoretical results with experimental data of fission fragments and evaporation residue nuclei in a very wide set of nuclear reactions.

In figure B.18 it is possible to observe the trend of the damping function as a function of T , where the nuclear temperature T is connected with the excitation energy E^* by the relation $T = \sqrt{\frac{E^*}{a}}$. For example, in Fig. B.18 (a) the changing of $h(T)$ from the maximum value (close to 1) to $1/2$ corresponds to the excitation energy $E^* = aT^2$ that, for example, in the case of a reaction leading to the $^{274}\text{Hs}^*$ CN is about 37 MeV. Moreover, $h(T)$ reaches the value 0.1 when the nuclear temperature is about 1.83 MeV; this value corresponds to the excitation energy E^* of about 92 MeV. Therefore, the damping function $h(T)$ with the T_0 and d values that we use leads to a very soft damping function with respect the nuclear temperature and consequently with respect the excitation energy E_{CN}^* too. The use of the parameters $d = 0.3$ MeV and $T_0 = 1.16$ MeV in the damping function of the nuclear temperature is not an arbitrary and convenient choice for some specific nuclear reactions and compound nuclei, but it is an appropriate result obtained by investigation of a very wide set of heavy-ion reactions. In Fig. B.18 (b), $\ell_{1/2} = 20\hbar$ and $\Delta\ell = 3\hbar$ parameters reduce the $q(\ell)$ function from 0.9 to 0.1 in the (12-26) \hbar interval confirming the important role of the $q(\ell)$ damping function in determination of the effective fission barrier $B_{\text{fis}}(\ell, T)$. It is useful to note that the values of parameters d , T_0 , $\ell_{1/2}$ and $\Delta\ell$ used in the damping functions $h(T)$ and $q(\ell)$ are not changed in the study of heavy-ion reactions leading to heavy and superheavy nuclei as those considered in Table 1.

In our code the fission and particle decay widths Γ_{fis} and Γ_x are calculated by the formulas

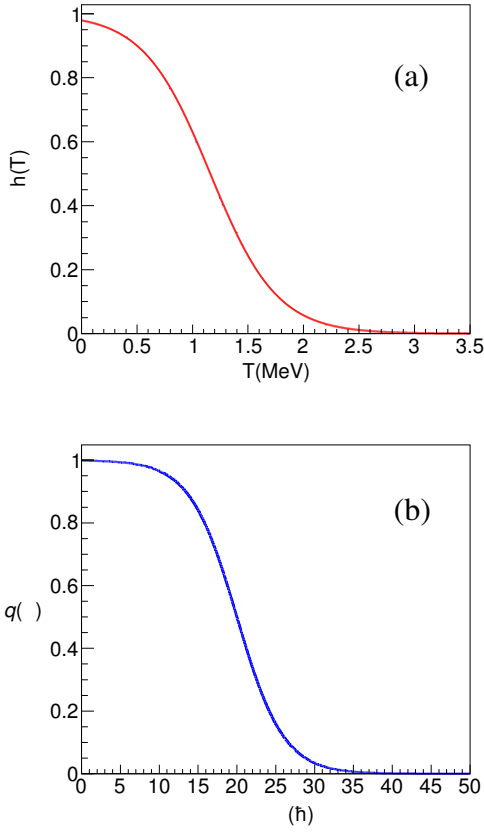


Figure B.18: (Color on-line) (a) The damping function $h(T)$ vs T nuclear temperature (full line) for $T_0 = 1.16$ MeV and $d = 0.3$ MeV. (b) The damping function $q(\ell)$ vs ℓ (dashed line) for $\ell_{1/2} = 20\hbar$ and $\Delta\ell = 3\hbar$ parameters.

$$\Gamma_{\text{fis}}(E, J) = \frac{1}{2\pi\rho(E, J)} \int_0^{E-E_{\text{sad}}(J)} \rho_{\text{fis}}(E - E_{\text{sad}}(J) - \epsilon, J) \times T_{\text{fis}}(E - E_{\text{sad}}(J) - \epsilon) d\epsilon, \quad (\text{B.1})$$

and

$$\Gamma_x(E, J) = \frac{1}{2\pi\rho(E, J)} \sum_{J'=0}^{\infty} \sum_{j=|J'-J|}^{J'+J} \int_0^{E-B_x} \rho_x(E - E_x - \epsilon, J') T_x^{\ell, j}(\epsilon) d\epsilon, \quad (\text{B.2})$$

where the subscript *fis* and *x* refer, respectively, to the fission process and particle-*x* emission channels (neutron, proton, α , and γ), and primes are used to mark an intermediate excited nucleus after particle emission and $E_{\text{sad}}(J)$ is the energy of the decaying nucleus at the saddle point with angular momentum ℓ and total spin J . It is known that a nucleus at the saddle point have a strong prolate deformation with the angular momentum vector perpendicular to the symmetry axis and therefore the rotational contribution to $E_{\text{sad}}(J)$ is given by

$$\hbar^2 J(J+1)/2(\mathcal{J}_{\perp})_{\text{sad}}. \quad (\text{B.3})$$

In the case of the yrast state (equilibrium state of the residual nucleus reached after particle or gamma emission), the formation is usually slight and the shape may be prolate, oblate or even triaxial. For prolate yrast deformation, we assume rotation around the axis perpendicular to the symmetry axis and retain expression (B.4) to calculate the rotational energy contribution. In the case of the oblate deformation, however, the nucleus is assumed to rotate around its symmetry axis and the rotational energy contribution to the potential-energy surface becomes

$$\hbar^2 J(J+1)/2(\mathcal{J}_{\perp})_{\text{yr}}, \quad (\text{B.4})$$

therefore, the effective moment of inertia \mathcal{J}_{eff} is defined by the relation

$$\frac{1}{\mathcal{J}_{\text{eff}}} = \frac{1}{\mathcal{J}_{\parallel}} - \frac{1}{\mathcal{J}_{\perp}} \quad (\text{B.5})$$

In addition, in formulas (B.1) and (B.2) ρ , ρ_{fis} and ρ_x represent the collective level densities of the formed excited nucleus, the level density of the excited nucleus at the saddle point configuration for orbital angular momentum ℓ , and the level density of the reached subsequent excited nucleus after particle-*x* emission for orbital angular momentum ℓ , respectively. $T_x^{\ell, j}$ is an optical-model transmission coefficient for particle-*x* with angular momentum ℓ coupled with particle spin to give j , and the fission transmission coefficient T_{fis} in the Hill-Wheeler approximation is given by $T_{\text{fis}} = \{1 + \exp[-2\pi(E^* - E_{\text{sad}}(J) - \epsilon)/\hbar\omega]\}^{-1}$, with $\hbar\omega = 1$ MeV. In the case of involved high excitation energies, the fission transmission coefficient is practically equal to unity, and therefore the particular choice of the $\hbar\omega$ value is irrelevant for the result of calculation. The estimation of the effect of nuclear deformation at high spin values on the determination of the transmission coefficient was studied by [55]. The main effect of the deformation was found to consist in the shift of the transmission coefficient threshold toward lower energies. This shift is of the order of 1 MeV and may eventually lead to a substantial modification of the charged-particle emission close to the threshold, but should not be relevant for the fission cross section.

It is useful to observe that in formula (B.1) the calculation of Γ_{fis} fission width is characterized in the nominator by the level density ρ_{fis} of the excited nucleus that reaches the saddle point state with angular momentum ℓ and total spin J - weighted by the transmission coefficient T_{fis} - and in the denominator by the level density $\rho(E, J)$ of the same excited and rotating nucleus at the statistical equilibrated state with energy E and spin J , while in (B.2) the calculation of the Γ_x width for particle-*x* emission - weighted by the T_x transmission coefficient - is characterized in the nominator by the level density $\rho_x(E - B_x - \epsilon, J')$ of the intermediate excited nucleus reached after emission of one particle-*x* (weighted by the T_x transmission coefficient) and in the denominator by the level density $\rho(E, J)$ of the decaying excited nucleus.

In formulas (B.1) and (B.2) the Coulomb barriers for emission of light particles are obtained by [56], the transmission coefficients are obtained by the routine SCAT2 [57], and binding

energies for light particles are calculated using masses recommended by [49] whenever available, otherwise theoretical predictions of [58] are used. The parity selection rules are also considered in calculation.

Figure B.19 shows the sensitivity of the method in calculation of survival probability $W_{\text{sur}}(E^*)$ for the $^{16}\text{O}+^{204}\text{Pb}$ reaction leading to the heavy ^{220}Th CN when a relevant change of $\pm 5\%$ of asymptotic level density parameter \bar{a} in formula (12) is considered (see panel (a)), and also the sensitivity of $W_{\text{sur}}(E_{\text{CN}}^*)$ when a relevant change of $\pm 5\%$ of the γ parameter in the exponent term of formula (12) is considered (see panel (b)) accounting for the rate of wash out of the shell effects with the excitation energy. For example, at $E_{\text{CN}}^* = 38$ MeV of excitation energy, $W_{\text{sur}}(E_{\text{CN}}^*)$ changes by a factor 1.2 with the relevant change of 5% in the \bar{a} value from 20.68 to 21.71 MeV^{-1} or from 20.68 to 19.65 MeV^{-1} (see panel (a)); the change of $W_{\text{sur}}(E_{\text{CN}}^*)$ with the changing of $\pm 5\%$ is by a factor 1.1.

Analogously, the panel (a) of Fig. B.20 shows an accentuate sensitivity in calculation of $W_{\text{sur}}(E_{\text{CN}}^*)$ for the $^{26}\text{Mg}+^{248}\text{Cm}$ reaction leading to the superheavy ^{274}Hs CN when the same change of $\pm 5\%$ of the \bar{a} parameter is considered; in this case of superheavy nucleus with $Z=108$ and $A=274$, at $E_{\text{CN}}^* = 44$ MeV of excitation energy, the observed $W_{\text{sur}}(E_{\text{CN}}^*)$ values change by a factor of about 2.0 or 1.3 when \bar{a} changes from 25.76 to 24.47 MeV^{-1} , or from 25.76 to 27.05 MeV^{-1} , respectively. The panel (b) of Fig. B.20 shows, instead, that a change of $\pm 5\%$ in the γ parameter value produces a variation of $W_{\text{sur}}(E_{\text{CN}}^*)$ at $E_{\text{CN}}^* = 44$ MeV by a factor of about 1.5-1.3 for the $^{274}108$ superheavy nucleus, respectively. The present discussion is only made to show the sensitivity of the method for the calculation of $W_{\text{sur}}(E_{\text{CN}}^*)$ for various considered compound nuclei and nuclear reactions, but we always use in our calculation the standard parameters present in \bar{a} , damping function of shell effects with E_{CN}^* in the determination of the level density parameter a , damping functions of the shell effects with E_{CN}^* and angular momentum ℓ , on the fission barrier, respectively. Never we use free parameters in order to study any mass asymmetric and almost symmetric reactions leading to heavy and superheavy nuclei.

By regarding $K_{\text{rot}}^{\text{adiab}}(E^*)$ and $K_{\text{vibr}}^{\text{adiab}}(E^*)$ collective enhancement coefficients present in formula (16) for all studied reactions are used. The vibrational enhancement coefficient is determined by the relation [59, 60]

$$K_{\text{vibr}}^{\text{adiab}}(E^*) = \exp \left[1.69 \left(\frac{3m_0 A}{4\pi\sigma_{\text{l.d.}}} \frac{C_{\text{l.d.}}}{C} \right)^{\frac{2}{3}} T^{\frac{4}{3}} \right] \quad (\text{B.6})$$

where $\sigma_{\text{l.d.}} = 1.2 \text{ MeV fm}^{-2}$ is the surface tension value in the liquid-drop model, m_0 is the nucleon mass, A is the mass number of the formed excited nucleus, and the $C/C_{\text{l.d.}}$ ratio is related to the different characteristics between the restoring force coefficient of the excited nucleus and the corresponding rigidity coefficient of the liquid-drop model. In our calculation $C = C_{\text{l.d.}}$ (liquid-drop value of rigidity coefficient) was used for all reactions forming CN. The rotational enhancement coefficient is determined by one of the following relations

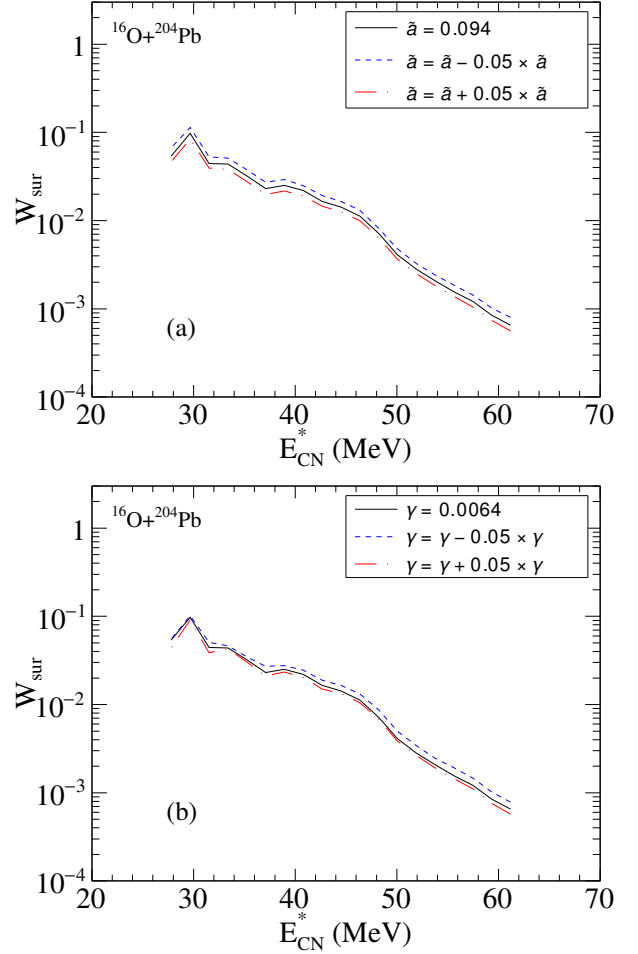


Figure B.19: Survival probability W_{sur} vs E_{CN}^* for the $^{16}\text{O}+^{204}\text{Pb}$ reaction leading to the heavy ^{220}Th CN. Panel (a) represents W_{sur} computed when \bar{a} parameter was changed by $\pm 5\%$ (dashed line for -5% and dash-dotted line for $+5\%$; full line for the standard parameter $\bar{a} = 0.094 \times A$). Panel (b) represents W_{sur} computed when γ parameter was changed by $\pm 5\%$ (dashed line for -5% and dash-dotted line for $+5\%$; full line for the standard parameter $\gamma = 0.0064 \text{ MeV}^{-1}$).

$$K_{\text{rot}}^{\text{adiab}}(E^*) = \begin{cases} 1, & \text{for spherical nuclei,} \\ \sigma_{\perp}^2, & \text{for axially and mirror-symmetric nuclei,} \\ 2\sigma_{\perp}^2, & \text{for axially-symmetric and} \\ & \text{mirror-asymmetric nuclei,} \\ \sqrt{\frac{\pi}{2}}2\sigma_{\perp}^2\sigma_{\parallel}, & \text{for ellipsoidal } (D_2) \text{ symmetry of nuclei,} \\ \sqrt{8\pi}2\sigma_{\perp}^2\sigma_{\parallel}, & \text{for nuclei possessing no symmetry.} \end{cases} \quad (\text{B.7})$$

In formula B.7, the spin-dependent parameters $\sigma_{\perp} = (\mathcal{J}_{\perp}T/\hbar^2)^{\frac{1}{2}}$ and $\sigma_{\parallel} = (\mathcal{J}_{\parallel}T/\hbar^2)^{\frac{1}{2}}$ are related to the perpendicular \mathcal{J}_{\perp} and parallel \mathcal{J}_{\parallel} moments of inertia of the deformed nucleus [60], respectively

$$\mathcal{J}_{\perp} = \frac{2}{5}m_0r_0^2A^{\frac{5}{3}}\left(1 + \frac{1}{3}\beta\right) \quad (\text{B.8})$$

$$\mathcal{J}_{\parallel} = \frac{6}{\pi^2} \langle m^2 \rangle a \left(1 - \frac{2}{3}\beta\right) \quad (\text{B.9})$$

where β is the deformation parameter of the nucleus and it represents the parameter of the internal nuclear quadrupole moment.

In order to calculate the collective level density in the non-adiabatic approach $\rho_{\text{coll}}^{\text{non-adiab}}(E^*, J)$ - necessary when the CN is formed at higher E_{CN}^* excitation energies - we used a damped collective enhancement function $q(E^*, \beta)$ with the aim to account the coupling of the collective to intrinsic degrees of freedom due to the nuclear viscosity because while it is acceptable to treat collective modes within the adiabatic approximation at low energies, it is rather unlikely that at high energies the adiabatic assumption still holds, due to the coupling of the elementary modes to the collective ones. So we introduce a certain general function for damping collective effects in the level density, depending strongly on the excitation energy and deformation of the nucleus. This is expressed in a decrease of the collective enhancement coefficient $K_{\text{coll}}(E^*)$ when the excitation energy increases; therefore, the following expression was assumed [61, 62]

$$K_{\text{coll}}^{\text{non-adiab}}(E^*) = \left\{ [K_{\text{rot}}^{\text{adiab}}(E^*) - 1]q(E^*, \beta) + 1 \right\} \times \left\{ [K_{\text{vibr}}^{\text{adiab}}(E^*) - 1]q(E^*, \beta) + 1 \right\} \quad (\text{B.10})$$

where

$$q(E^*, \beta) = \exp[-E^*/E_1(\beta)]. \quad (\text{B.11})$$

The expression of damping function is used in the fission and neutron (or other light particles) emission channels in the same way [63]. In formula (B.11) the following expression for $E_1(\beta)$ was assumed

$$E_1(\beta) \cong 170 \times A^{\frac{1}{3}}\beta^2 \quad (\text{B.12})$$

in order to reach the better agreement between calculated values of fission cross sections and experimental ones for a wide set of nuclear reactions leading to compound nuclei lighter than lead,

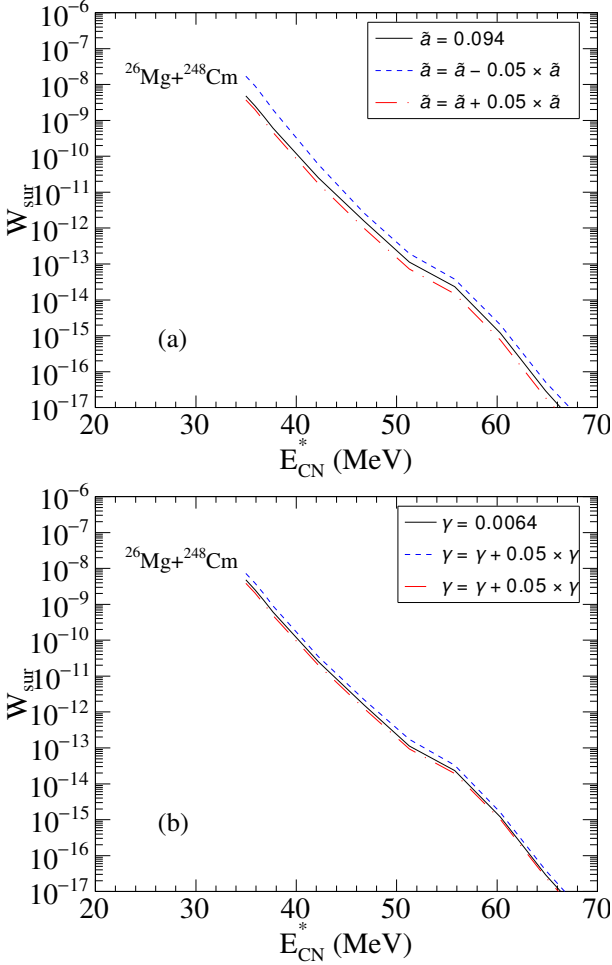


Figure B.20: As Fig. B.19, but for the $^{26}\text{Mg}+^{248}\text{Cm}$ reaction leading to the superheavy ^{274}Hs CN.

preactinide and actinide compound nuclei, and also for nuclei with $Z > 100$. At the same time, the comparison between theoretical estimation of evaporation residue cross sections and experimental determinations have contributed to the choice of the damping function $q(E^*, \beta)$ to the K_{coll} collective enhancement coefficient given in formula (B.11) together with the expression (B.12). The consequence of the quadratic dependence of $E_1(\beta)$ on β (see relation (B.12)) is that the damping at the saddle point ($\beta \approx 0.6 - 0.8$) is negligible in the high E^* excitation energy region, while the deviations of $q(E^*, \beta)$ from unity are already considerable for the neutron channel ($\beta \approx 0.2 - 0.3$) at low E^* excitation energy values.

As an example of sensitivity of our refined model and procedures, we present in Fig. B.21 the calculated neutron energy spectrum of some emitted neutrons at various steps, starting from the $^{288}114$ CN at $E_{\text{CN}}^* = 35.89$ MeV of excitation energy formed in the $^{48}\text{Ca} + ^{240}\text{Pu}$ reaction along the deexcitation cascade. In Fig. B.22 we present the calculated energy spectra of neutron, proton, and α -particle emitted from the mentioned $^{288}114$ CN ($E_{\text{CN}}^* = 40.06$ MeV) at the first step of the cascade.

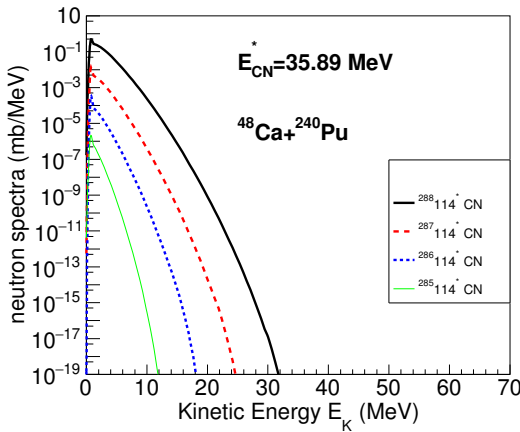


Figure B.21: (Color on-line) Energy spectra of neutrons emitted at various steps of the deexcitation cascade starting from the $^{288}114$ CN at $E_{\text{CN}}^* = 35.89$ MeV of excitation energy by the $^{48}\text{Ca} + ^{240}\text{Pu}$ reaction: thick full line for the first neutron emitted from $^{288}114$ CN*, dashed lines for the first neutron emitted from $^{287}114^*$, dotted line for the first neutron emitted from $^{286}114^*$ and thin full line for the first neutron emitted from $^{285}114^*$.

Formula (9) of our manuscript describes the effective fission barrier obtained as the sum of the macroscopic fission barrier $B_{\text{fis}}^m(\ell)$ depending only on the angular momentum ℓ and the microscopic correction δW due to the shell effects. In our calculation $h(T)$ and $q(\ell)$ are the damping functions of the nuclear shell correction δW by the increase of the excitation energy E^* and angular momentum ℓ , respectively, and then the determination of the effective fission barrier $B_{\text{fis}}(T, \ell)$ for each excited nucleus formed at various steps along the deexcitation cascade of the compound nucleus (CN) is a function of T and ℓ . The parameters used to determine the level density, the effective fission barrier and the damping function have been extensively validated during the long-term investigation over hundreds considered nuclear reactions (from strongly mass asymmetric reac-

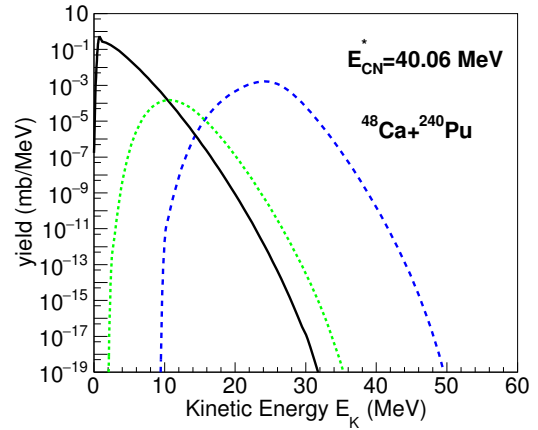


Figure B.22: Energy spectra of n, p, α emitted from the $^{288}114$ CN* at $E_{\text{CN}}^* = 40.06$ MeV of excitation energy by the $^{48}\text{Ca} + ^{240}\text{Pu}$ reaction: full line for the first emitted neutron, dotted line for the first emitted proton, dashed line for the first emitted α -particle.

tions to almost symmetric ones) leading to heavy and super-heavy nuclei.

References

- [1] F. Michel, G. Reidemeister, and S. Ohkubo, Phys. Rev. Lett. 89 (2002) 152701.
- [2] H. Q. Zhang *et al.*, Phys. Rev. C 81 (2010) 034611.
- [3] H. Esbensen, Phys. Rev. C 81 (2010) 034606.
- [4] A. K. Nasirov *et al.*, Phys. Rev. C 79 (2009) 024606.
- [5] G. Fazio *et al.*, Mod. Phys. Lett. A 20 (2005) 391.
- [6] G. Giardina *et al.*, Int. J. Mod. Phys. E 19 (2010) 882.
- [7] A. K. Nasirov *et al.*, Phys. Rev. C 84 (2011) 044612.
- [8] A. K. Nasirov *et al.*, Eur. Phys. J. A 49 (2013) 147.
- [9] G. Fazio *et al.*, J. Phys. Soc. JPN. 77 (2008) 124201.
- [10] K. Kim *et al.*, Phys. Rev. C 91 (2015) 064608.
- [11] A. K. Nasirov *et al.*, Journal of Physics: Conference Series 205 (2010) 012018.
- [12] G. Mandaglio *et al.*, Phys. Rev. C 86 (2012) 064607.
- [13] G. Mandaglio *et al.*, EPJ Web of Conferences 96 (2015) 01016.
- [14] G. Giardina *et al.*, Journal of Physics: Conference Series 282 (2011) 012006.
- [15] G. N. Knyazheva *et al.*, Phys. Rev. C 75 (2007) 064602.
- [16] G. Fazio *et al.*, Eur. Phys. J. A 22 (2004) 75.
- [17] G. Fazio *et al.*, Phys. Rev. C 72 (2005) 064614.
- [18] Avazbek Nasirov, Akira Fukushima, Yuka Toyoshima, Yoshihiro Aritomo, Akhtam Muminov, Shuhrat Kalandarov, Ravshanbek Utamuratov, Nucl. Phys. A 759, (2005) p.342-369.
- [19] A. J. Sierk, Phys. Rev. C 33 (1986) 2039.
- [20] A. Sobczewski, K. Pomorski, Prog. Part. Nucl. Phys. 58 (2007) 292.
- [21] W. Loveland, Eur. Phys. J. A 51 (2015) 120.
- [22] M. G. Itkis *et al.*, AIP Conf. Proc. 853 (2006) 231.
- [23] M. G. Itkis *et al.*, Nucl. Phys. A 787 (2007) 150c.
- [24] G. G. Adamian *et al.*, Phys. Rev. C 68 (2003) 034601.
- [25] N. Wang *et al.*, Phys. Rev. C 84 (2011) 061601.
- [26] L. Zhu *et al.*, Phys. Rev. C 89 (2014) 024615.
- [27] G. Fazio *et al.*, in *Proceedings of the International Symposium New Projects and Lines of Research in Nuclear Physics, Messina, Italy, 24-26 October 2002*, edited by G. Fazio and F. Hanappe (World Scientific, Singapore, 2003), pp. 258-271.
- [28] A. K. Nasirov *et al.*, in *Proceedings of the Symposium Nuclear Clusters, Rauschholzhausen, Germany, 5-9 August 2002*, edited by R. V. Jolos and W. Scheid (EP Systema, Debrecen, 2003), pp. 415-426; Acta Phys. Hung. A 19 (2004) 109.

- [29] Y. Aritomo and M. Ohta, Nucl. Phys. A 744 (2004) 3.
- [30] A.K. Nasirov *et al.*, Phys. Lett. B 686 (2010) 72.
- [31] G. Mandaglio *et al.*, EPJ Web of Conferences 38 (2012) 01001.
- [32] V. Zagrebaev, W. Greiner, Phys. Rev. C 78 (2008) 034610.
- [33] A. Anastasi *et al.*, Acta Physica Polonica B 8 (2015) 583.
- [34] R. Yanez, W. Loveland *et al.*, Phys. Rev. Lett. 112 (2014) 152702.
- [35] M. Kowal *et al.*, Phys. Rev. C 82 (2010) 014303.
- [36] H.A. Kramers, Physica 7 (1940) 284.
- [37] P. Möller, J.R. Nix, W.D. Myers, and W.J. Swiatecki, Atomic Data and Nuclear Data Tables 59, 185 (1995).
- [38] I. Muntian, Z. Patyk, and A. Sobieczewski, Phys. At. Nucl. 66 (2003) 1015.
- [39] P. Möller *et al.*, Phys. Rev. C 79, 064304 (2009).
- [40] J. Dvorak *et al.*, Phys. Rev. Lett. 100 (2008) 132503.
- [41] A. V. Ignatyuk, G. N. Smirenkin, and A. S. Tishin, Sov. J. Nucl. Phys. 21 (1975) 255.
- [42] A. D'Arrigo, G. Giardina, M. Herman, A. V. Ignatyuk, and A. Taccone, J. Phys. G: Nucl. Part. Phys. 20 365 (1994).
- [43] G. Fazio *et al.*, J. Phys. Soc. Jpn. 72 (2003) 2509.
- [44] G. Fazio *et al.*, Eur. Phys. Jour. A19, (2004) 89.
- [45] R.V. Jolos, A.I. Muminov, A.K. Nasirov, Yad. Fiz. 44, 357 (1986); Sov. J. Nucl. Phys. 44, 228 (1986).
- [46] G.G. Adamian, R.V. Jolos, A.K. Nasirov, Yad. Fiz. 55 (1992) 660, Sov. J. Nucl. Phys. 55, 366 (1992).
- [47] A.K. Nasirov *et al.*, Eur. Phys. J. A 34, 325 (2007).
- [48] N.V. Antonenko *et al.*, Phys. Rev. C 51, 2635 (1995).
- [49] G. Audi and A. H. Wapstra, Nucl. Phys. A595 (1995) 409.
- [50] C.Y. Wong, Phys. Rev. Lett. 31, 766 (1973).
- [51] A.B. Migdal, Theory of the Finite Fermi Systems and Properties of Atomic Nuclei, Moscow, Nauka, 1983.
- [52] S. Raman, C.H. Malarkey, W.T. Milner, C.W. Nestor, Jr., and P.H. Stelson, Atomic Data and Nuclear Data Tables 36 (1987) 1.
- [53] R. H. Spear, Atomic Data and Nuclear Data Tables 42 (1989) 55.
- [54] A.R. Junghans *et al.*, Nucl. Phys. A629 635 (1998)
- [55] S. E. Vigdor and H. J. Karwowski, Phys. Rev. C26 (1982) 1068.
- [56] A. R. Barnett *et al.*, Computer Phys. Communications 8 (1974) 377.
- [57] O. Bersillon, SCAT2, Optical Model Code, CEA Bruyeres-le-Chatel, France (1979).
- [58] P. Möller and J. R. Nix, Report of the Theoretical Division, Los Alamos National Laboratory, Los Alamos NM87545 (1986).
- [59] S. Yu. Platonov *et al.*, Nucl. Phys. A 503 (1989) 461.
- [60] A. V. Ignatyuk *et al.*, Sov. J. Nucl. Phys. 29 (1979) 450.
- [61] A. V. Ignatyuk *et al.*, Sov. J. Nucl. Phys. 30 (1979) 626.
- [62] G. Hansen and A. S. Jensen, Nucl. Phys. A 406 (1983) 236.
- [63] E. M. Rastopchin *et al.*, Sov. J. Nucl. Phys. 49 (1989) 15.